Ocean Sci. Discuss., doi:10.5194/os-2016-76, 2016
Manuscript under review for journal Ocean Sci.
Published: 17 October 2016

Ocean Science
Discussions
Open Access
EGU

Characteristics and causes of Deep Western Boundary Current transport variability at 34.5°S during 2009-2014

Christopher S. Meinen[1], Silvia L. Garzoli[2,1], Renellys C. Perez[2,1], Edmo Campos[3,2], Alberto R. Piola[4,5], Maria Paz Chidichimo[4, 5, 6], Shenfu Dong[1], and Olga Sato[3]

[1]Atlantic Oceanographic and Meteorological Laboratory, Miami, Florida
[2]Cooperative Institute for Marine and Atmospheric Studies, University of Miami, Miami, Florida
[3]University of São Paulo, São Paulo, Brazil
[4]Servicio de Hidrografía Naval, Buenos Aires, Argentina
[5]Universidad de Buenos Aires, Buenos Aires, Argentina
[6]Consejo Nacional de Investigaciones Científicas y Técnicas (CONICET), Argentina

Abstract:

The Deep Western Boundary Current (DWBC) at 34.5°S in the South Atlantic carries a significant fraction of the cold deep limb of the Meridional Overturning Circulation (MOC), and therefore its variability affects both the meridional heat transport and the regional and global climate. Nearly six years of observations from a line of pressure-equipped inverted echo sounders (PIES) have yielded an unprecedented data set for studying the characteristics of the time-varying DWBC volume transport at 34.5°S. Furthermore, the horizontal resolution of the observing array was greatly improved in December 2012 with the addition of two current-and-pressure-equipped inverted echo sounders (CPIES) at the midpoints of three of the existing sites. Regular hydrographic sections along the PIES/CPIES line confirm the presence of recently-ventilated North Atlantic Deep Water carried by the DWBC. The time-mean absolute geostrophic transport integrated within the DWBC layer, defined between 800-4800 dbar, and within longitude bounds of 51.5°W to 44.5°W is -15 Sv (1 Sv = 10^6 m^3 s^{-1}; negative indicates southward flow). The observed peak-to-peak range in volume transport using these integration limits is from -89 Sv to +50 Sv, and the temporal standard deviation is 23 Sv. Testing different vertical integration limits based on time-mean water-mass property

Ocean Sci. Discuss., doi:10.5194/os-2016-76, 2016
Manuscript under review for journal Ocean Sci.
Published: 17 October 2016

levels yields small changes to these values, but no significant alteration to the character of the transport time series. The time-mean southward DWBC flow at this latitude is confined west of 49.5°W, with recirculations dominating the flow further offshore. As with other latitudes where the DWBC has been observed for multiple years, the time variability greatly exceeds the time-mean, suggesting the presence of strong coherent vortices and/or Rossby Wave-like signals propagating to the boundary from the interior.

Introduction:

In the South Atlantic at 34.5°S the Deep Western Boundary Current (DWBC) is thought to carry the majority of the cold deep limb of the Meridional Overturning Circulation (MOC) southward toward the Southern Ocean. The MOC system dominates the north-south transport of heat and salt in the Atlantic Ocean (e.g. Trenberth et al. 2001; Ganachaud and Wunsch 2003; Johns et al. 2011), and studies using numerical climate models suggest significant connections between variations in the MOC and changes in socially relevant quantities such as continental precipitation patterns, hurricane intensification, and regional sea level (e.g. Vellinga and Wood 2002; Stouffer et al. 2006; Latif et al. 2007; McCarthy et al. 2015; Lopez et al. 2016). The pathways that the DWBC, and the lower limb of the MOC, take as they pass through the South Atlantic are not as well understood as in the North Atlantic. In a recent paper, Garzoli et al. (2015) used all available WOCE and CLIVAR-era hydrographic sections including dissolved oxygen and chlorofluorocarbon (CFC) data, Argo float profile data, and two different analyses of the Ocean general circulation model For the Earth Simulator (OFES) to trace the time-mean pathways of the DWBC through the South Atlantic. Together with other

Ocean Sci. Discuss., doi:10.5194/os-2016-76, 2016
Manuscript under review for journal Ocean Sci.
Published: 17 October 2016

historical analyses, their results show that the DWBC crosses 5°S as a narrow western boundary current, and it becomes dominated by eddies further south around 8°S-11°S, consistent with earlier mooring observations (Dengler et al. 2004; Schott et al. 2005). Previous work has suggested that when this very energetic eddying flow reaches the Vitória-Trindade Ridge at about 20°S, the mean flow appears to follow two different pathways, with a significant fraction (estimates ranging from 3 to 12 Sv) flowing eastward across the Mid-Atlantic Ridge toward the African continent (e.g. Zangenberg and Siedler 1998; Arhan et al. 2003; Hogg and Thurnherr 2005; van Sebille et al. 2012) and the remainder flowing southward along the western boundary hugging the South American continental slope. The recent analysis of ship sections of CFC, oxygen and salinity by Garzoli et al. (2015) clearly demonstrates that the strongest pathway in the South Atlantic south of about 22°S for recently-ventilated North Atlantic Deep Water (NADW), the primary water mass carried in the DWBC, is along the western boundary in the form of a narrow boundary current similar to what is found in most of the North Atlantic. That study suggests that only a small fraction, about 20%, of the DWBC volume transport flows eastward near 20°S, consistent with Arhan et al. (2003) and van Sebille et al. (2012). The Garzoli et al. (2015) study, however, focused primarily on the time-mean circulation pattern and provides little information about the time variability of the DWBC flow, which is the focus of the present study.

Variations of the MOC and the DWBC have historically been studied mostly in the North Atlantic (e.g. Meinen et al. 2013a; Perez et al. 2015; Srokosz and Bryden 2015; Frajka-Williams et al. 2016; and citations therein). This has mostly been a matter of

Ocean Sci. Discuss., doi:10.5194/os-2016-76, 2016
Manuscript under review for journal Ocean Sci.
Published: 17 October 2016

convenience and proximity, not a reflection on scientific importance, as theoretical work and numerical models have suggested that variations in the South Atlantic may be critical to the stability and flow of the overall MOC system (e.g. Dijkstra 2007; Drijfhout et al. 2011; Garzoli and Matano 2011; Garzoli et al. 2013; Buckley and Marshall 2016). Only in the past few years have observations been collected to study the MOC and/or the DWBC in the South Atlantic region, beginning with repeated upper ocean expendable bathythermograph (XBT) transects (e.g. Garzoli and Baringer, 2007; Dong et al. 2009) and full-depth hydrographic sections (e.g. Lumpkin and Speer 2003, 2007; Bryden et al. 2011), and later adding continuous moored observations at a few locations including 11°S (Hummels et al. 2015) and 34.5°S (Meinen et al. 2012; Meinen et al. 2013b). Gridded data sets from Argo float profiles in the upper 2000 m of the water column and satellite altimetry measurements have also been brought to bear on the meridional flows in the South Atlantic (e.g. Schmid 2014; Dong et al. 2015; Majunder et al. 2016), providing important information about latitudinal variations of the MOC. Note that most of these systems focus only on the volume transport in the upper water column, and do not directly observe the DWBC (e.g. XBT, Argo).

True continuous time series observations of the time varying deep limb of the MOC, the DWBC, are very limited in the South Atlantic. In terms of continuous measurements of absolute volume transports, in the scientific literature there are essentially only a few years of observations (2000-2004; 2013-2014) at 11°S (e.g. Hummels et al. 2015), and about one year of observations (2009-2010) at 34.5°S (Meinen et al. 2012). The WOCE Deep Basin Experiment (DBE) in the early 1990s, used current meters to measure the

Ocean Sci. Discuss., doi:10.5194/os-2016-76, 2016
Manuscript under review for journal Ocean Sci.
Published: 17 October 2016

components of the deep and abyssal flows at 20°S and 30°S with an emphasis on Antarctic Bottom Water (AABW) transports, but did not estimate the integrated DWBC volume transports (Hogg et al. 1999). The purpose of this paper is to extend the DWBC record at 34.5°S to five and a half years (2009-2014), examining daily to monthly changes as well as variability on seasonal and longer time scales. The paper examines possible causes for the largest observed DWBC variations, and puts them into context through comparisons with previous DWBC findings at other latitudes, as well as with numerical model output.

Data and Methods:

The Southwest Atlantic MOC ("SAM") array was first deployed at 34.5°S in March 2009 to capture the meridional flow of the western boundary currents, with the primary aim of making long-term measurements of the western boundary flows associated with the MOC (Meinen et al. 2012; Meinen et al. 2013b). The ultimate long-term goal was also for the SAM array to be a cornerstone for the South Atlantic MOC Basin-wide Array ("SAMBA") at 34.5°S, which is coming to fruition with parallel deployments occurring on the eastern boundary in 2013 and 2014 (e.g. Ansorge et al. 2014). The SAM array involves four pressure-equipped inverted echo sounders (PIES) deployed at depths ranging from about 1300 m down to about 4700 m, and extending roughly 650 km offshore from the outer edge of the continental shelf (see Table 1 and Figure 1). Note that the Site B PIES (see Figure 1) malfunctioned in 2010 and was lost during a recovery attempt in July 2011, so there is a roughly one-year gap at that site in 2010-2011.

Ocean Sci. Discuss., doi:10.5194/os-2016-76, 2016
Manuscript under review for journal Ocean Sci.
Published: 17 October 2016

124

125 The array location was selected to be just north of the northern edge of the meander
126 window of the Brazil-Malvinas Confluence (e.g. Gordon and Greengrove 1986; Olson et
127 al. 1988; Garzoli 1993; Goni et al. 1996, 2011; Lumpkin and Garzoli 2011) based on
128 altimeter, sea surface temperature (SST), and surface drifting buoy measurements.
129 Depending on the precise indicator of the Brazil-Malvinas Confluence selected, the
130 seasonal movement of the Brazil-Malvinas Confluence is characterized either by
131 meridional shifts centered near 38.5°S (e.g. Matano 1993; Lumpkin and Garzoli 2011) or
132 by pivots around a fixed point located near 39.5°S, 53.5°W, changing its orientation from
133 N-S in austral winter to NW-SE in austral summer (Saraceno et al. 2004). The
134 meridional extremes in the Confluence location (denoted by sharp horizontal SST
135 gradients) are typically found in February and August, as can be seen in SST maps
136 (Figure 1, right panels).

137

138 Based on recommendations from the broad South Atlantic Meridional Overturning
139 Circulation (SAMOC) Initiative (see www.aoml.noaa.gov/phod/SAMOC_international/),
140 the PIES array was complemented in December 2012 with two current-and-pressure-
141 equipped inverted echo sounders (CPIES) as part of the parallel South Atlantic MOC-
142 Brazil project ("SAMOC-Br"). These CPIES instruments were deployed near the
143 midpoints of three of the existing PIES moorings (Figure 1) in order to provide better
144 horizontal resolution across the western boundary currents.

145

Ocean Sci. Discuss., doi:10.5194/os-2016-76, 2016
Manuscript under review for journal Ocean Sci.
Published: 17 October 2016

146 The analysis of PIES data has become more commonplace within the scientific
147 community over the past few decades, and their use to study the DWBC and the MOC in
148 both the North and South Atlantic has been well documented (e.g., Meinen et al. 2006;
149 Meinen et al. 2012; Meinen et al. 2013a,b). Therefore, the PIES analysis methods will
150 only be summarized here briefly, with the remainder of the methodology details left to
151 the references cited.
152
153 A PIES makes two measurements every hour: 1) the bottom pressure; and 2) the vertical
154 round-trip travel time required for a 12 kHz acoustic pulse to travel from the bottom
155 moored instrument up to the sea surface and back. The bottom pressure measurement is
156 made with a highly precise Paros pressure gauge (e.g. Watts and Kontoyiannis 1990;
157 Donohue et al. 2010), while the round-trip travel time is determined using a transducer
158 and a high quality crystal clock (e.g. Rossby 1969; Watts and Rossby 1977; Tracey and
159 Watts 1986). The travel time measurements from each PIES are calibrated into daily,
160 full-water-column profiles of temperature, salinity and specific volume anomaly via
161 hydrography-derived look-up tables using the Gravest Empirical Mode (GEM) technique
162 (e.g. Meinen and Watts 2000). The application of the GEM method to the PIES in the
163 SAM array was first done in Meinen et al. (2012)[1]; that study demonstrated that the
164 measured travel times were accurate to roughly 4.4% of the observed range when
165 compared with concurrent CTD profile data. That study also showed that the signal-to-
166 noise ratio (SNR) for the GEM look-up tables was around 20 for depths within the main

[1] Note: It was recently discovered that, due to a coding mistake, the time-varying bottom-pressure derived term in the absolute velocity in the 2012 study was added with the incorrect sign. The full time series has been recomputed for the present study. Although the character of the absolute transport time series changes due to this mistake, the major results of the earlier study were not impacted.

Ocean Sci. Discuss., doi:10.5194/os-2016-76, 2016
Manuscript under review for journal Ocean Sci.
Published: 17 October 2016

thermocline/halocline, and decreased to around 1-3 below 2000 dbar. The decreased SNR below 2000 dbar is a result of both a decreased correspondence between the observed changes and the empirical 'mode' captured by the GEM technique, and the much smaller signals themselves at these depths. Because the deep vertical shear (of density as well as horizontal velocity) is generally quite weak in this region – this does not represent a serious limitation for the purposes of this study.

Vertically integrating the specific volume anomaly profiles generated from the GEM fields and the PIES travel time measurements yields daily dynamic height anomaly profiles at each of the four instrument sites, and differences in dynamic height anomaly profiles between neighboring PIES sites provide relative geostrophic velocity profiles orthogonal to the line between the PIES (the 'baroclinic' component of the velocity; e.g. Meinen et al. 2006). Differences in bottom pressure from neighboring PIES sites provide absolute geostrophic velocity variability at the bottom that can be used to reference the relative velocity profiles (the 'barotropic' component of the velocity; e.g. Meinen and Watts 2000). Due to the well-known leveling problem, the time-mean absolute geostrophic velocity at the bottom cannot be determined from the bottom pressure differences (e.g. Donohue et al. 2010). The additional measurement of water velocity made by the CPIES can characterize the flow 50 m above the seafloor. However, given that the 2 CPIES were deployed much further apart than the typical velocity decorrelation length scale (e.g. Donohue et al. 2010), and given that there are only measurements at two locations (Figure 1), these velocity observations cannot solve the time-mean absolute velocity reference issue. As such those velocity measurements will not be discussed

Ocean Sci. Discuss., doi:10.5194/os-2016-76, 2016
Manuscript under review for journal Ocean Sci.
Published: 17 October 2016

190 further in this article, and for the purposes of this study the PIES and CPIES will be
191 treated interchangeably. As time variability is the focus of this paper, the time-mean
192 issue is not crucial for this study. However, to provide reasonable time-mean absolute
193 velocity profiles for discussion, the time-mean velocity from an ocean general circulation
194 model (the model is described in the next section) at 1500 dbar was added to the velocity
195 profiles created using the PIES data[2]. Note that only the *time-mean* velocity at only *1500*
196 *dbar* is used from the model for this purpose. All time variability from the PIES is
197 independent of the model, as is the time-mean velocity shear profile.
198
199 Most detailed testing of the PIES-GEM estimated velocities and transports has been done
200 in the North Atlantic where independent estimates were available at concurrent locations
201 – specifically for the DWBC this has been done at 26.5°N (e.g. Meinen et al. 2004, 2006,
202 2013a). Meinen et al. (2013a) compared daily PIES-derived transports to those
203 determined from dynamic height mooring data at 26.5°N and showed that DWBC
204 transports estimated from the two systems had a correlation of r = 0.96, and a root-mean-
205 square difference of 6 Sv. Furthermore, they showed that correlations for baroclinic
206 transports using an assumed level of no motion at 800 dbar were similarly high.
207 Unfortunately there are no independent absolute transport continuous time series
208 measurements for a similar comparison at 34.5°S as there are at 26.5°N. However, it can
209 be noted that the same types of instruments are used for both arrays, and the 34.5°S GEM

[2] Note that in the earlier Meinen et al. (2012) study the model mean velocity was added near the bottom; however, for this study the model velocity at 1500 dbar was used to avoid the significant ageostrophic velocity components in the model in the nearest-bottom grid cell. The results are not highly sensitive to this choice.

Ocean Sci. Discuss., doi:10.5194/os-2016-76, 2016
Manuscript under review for journal Ocean Sci.
Published: 17 October 2016

SNR of ~20 in the main thermocline depth range, and of 1–3 below 2000 dbar, are similar to what is observed at 26.5°N.

The GEM look-up tables used herein are based on a data set of 200 CTD profiles and 365 Argo profiles collected before the end of 2008. See Meinen et al. (2012) for more detail and an example GEM look-up table. Since the beginning of the SAM project, quasi-annual CTD sections have been collected along the PIES line both to provide concurrent calibration for the PIES travel times, and to observe finer-scale and better horizontal resolution water mass changes over time. These CTD data have not been incorporated into the GEM fields, and as such they represent an independent data set. For this study, CTD sections from July 2010, December 2010, July 2011, and December 2012 are averaged in a fairly simple manner solely to provide an overview of the major water masses. The CTDs collected right at the PIES sites were also used to calibrate the PIES travel times into travel time on a common pressure level (e.g. Meinen and Watts, 1998).

Numerical model output:

To aid in the interpretation of the observations from the PIES array at 34.5°S, output from a high quality, well-validated, numerical model was also used. The Ocean general circulation model For the Earth Simulator (OFES; e.g., Sasaki et al. 2008) was selected for this study. The OFES model is produced by the Japan Agency for Marine-Earth Science and Technology (JAMSTEC), and it is a massively parallelized implementation of the National Oceanic and Atmospheric Administration/Geophysical Fluid Dynamics Laboratory's Modular Ocean Model version 3 (MOM3). The model equations have been

Ocean Sci. Discuss., doi:10.5194/os-2016-76, 2016
Manuscript under review for journal Ocean Sci.
Published: 17 October 2016

discretized on a Mercator B-grid with 54 vertical z levels and a horizontal resolution of 0.1°. For the analysis presented here, model fields were provided by JAMSTEC on 3-day snapshot intervals with a 0.2° horizontal grid (i.e., every other grid point) during the period 1980 through 2006. The OFES model was spun up for 50 years using a monthly climatology derived from National Centers for Environmental Prediction-National Center for Atmospheric Research (NCEP/NCAR) reanalysis atmospheric fluxes (Masumoto et al. 2004), and it then was forced with daily mean NCEP/NCAR reanalysis data from 1950 to 2006 (Sasaki et al. 2008). To avoid remaining spin-up transients, only the output from the final 27 years of the run was used for this analysis. This model run was selected because it has previously been validated against both other models and the limited available observations in the South Atlantic (Dong et al. 2011; Perez et al. 2011; van Sebille et al. 2012; Garzoli et al. 2013; Garzoli et al. 2015).

Results and Discussion:

The time-mean absolute velocity section calculated from the PIES data during 2009-2014 via the methods described above shows the Brazil Current flowing southward between PIES Sites A and B between the surface and roughly 800 dbar, with the DWBC flowing southward below it (Figure 2a). These flows appear weak and smooth horizontally, however, keep in mind that because these velocities are calculated via the geostrophic method they represent a horizontal average between each pair of PIES sites – i.e. horizontal averages over 2-3 degrees of longitude. Also, along the SAM section west of ~49.5ºW the entire water column flows southward, so there is no obvious separation in the velocity section between the near-surface Brazil Current and the intermediate and

Ocean Sci. Discuss., doi:10.5194/os-2016-76, 2016
Manuscript under review for journal Ocean Sci.
Published: 17 October 2016

256 deep-water flows. Immediately offshore of these southward flows, recirculations to the
257 north in both the surface and deep layers are observed. Even further offshore, between
258 PIES Sites C and D, the flow turns southward once again.
259
260 The basic structure of the mean velocity section from the OFES model (Figure 2b)
261 compares favorably with the mean section from the data (Figure 2a), albeit with much
262 more horizontal structure. Additional horizontal information is available from the
263 PIES/CPIES array during the final two years – but before looking at that structure it is
264 instructive to first evaluate the time-mean velocities derived from the original four-PIES
265 array only during the final two-year period (Figure 2c). The roughly 2-year average is
266 similar to the 4 ½ year average (compare Figures 2a and 2c), with the upper layer
267 recirculation being slightly stronger and the deep ocean recirculation being slightly
268 weaker or even slightly southward at some depths during the shorter 2-year average.
269 Averaging the model velocity output between pairs of PIES to simulate the geostrophic
270 averaging (Figure 2d) yields a section that is qualitatively similar to the 2-year average
271 from the PIES, although there are some differences in intensity (compare Figures 2c and
272 2d).
273
274 Including the two CPIES records enhances the horizontal structure of the time-mean
275 section, with a more evident Brazil Current core, a stronger upper ocean recirculation
276 core, and a deep recirculation cell that extends to the bottom (Figure 2e). The model
277 velocity output averaged between the six sites (Figure 2f) is quite similar to the
278 PIES/CPIES velocity section, although the northward recirculation in the model is

Ocean Sci. Discuss., doi:10.5194/os-2016-76, 2016
Manuscript under review for journal Ocean Sci.
Published: 17 October 2016

weaker both near the surface and at depth. An important reminder: The time-mean model velocity at 1500 dbar was used to set the time-mean PIES flow at that pressure level as mentioned earlier (see dashed black lines in Figure 2), so there is perfect agreement between the PIES/CPIES time-mean velocity and the model velocity at 1500 dbar by construction. (Apparent differences at 1500 dbar are contouring artifacts only.)

As noted earlier, at 34.5°S, the western boundary flows in the upper and deep layers (Brazil Current and DWBC, respectively) overlay one another, such that the meridional velocities near the boundary are generally all southward from surface to bottom. One could attempt to use water mass properties to identify the level that bounds the base of the Brazil Current and the top of the DWBC, however as will now be shown, this is not particularly satisfying or successful at this location. Average vertical sections of temperature, salinity, dissolved oxygen, and neutral density (Figure 3) show obvious water mass layers, perhaps most clearly in the dissolved oxygen (Figure 3c). For the purposes of the discussion of deep-water flows in this paper, the following water mass definitions are used following Preu et al. (2013):

– Antarctic Intermediate Water (AAIW): salinity less than 34.25 psu;

– Upper Circumpolar Deep Water (UCDW): neutral density between 27.75 and 27.90 kg m^{-3} with dissolved oxygen values below 4.5 mL L^{-1};

– North Atlantic Deep Water (NADW): neutral density between 27.90 and 28.10 kg m^{-3} with salinity greater than 34.8 psu;

– Lower Circumpolar Deep Water (LCDW): neutral density between 28.06 and 28.20 kg m^{-3} with salinity less than 34.8 psu;

Ocean Sci. Discuss., doi:10.5194/os-2016-76, 2016
Manuscript under review for journal Ocean Sci.
Published: 17 October 2016

– Antarctic Bottom Water (AABW): potential temperature less than 0°C.

Based on these definitions, the layering of the water column along the SAM array clearly shows AAIW overlaying UCDW, which overlays NADW, which overlays LCDW, which finally overlays the AABW. These are most evident in the oxygen section (Figure 3c), with the enhanced oxygen values of the AAIW around 900 dbar, the NADW around 2800 dbar, and the AABW around 4800 dbar standing out from the comparatively lower oxygen waters of the UCDW and LCDW.

The time-mean locations of the main DWBC water mass interfaces demonstrate some rather surprising results when overlain on the time-mean meridional velocity section (Figure 4). Very near the continental slope the NADW is carried southward as one would expect in the DWBC, however immediately offshore the entire NADW layer is being carried *northward*, essentially heading back toward the northern formation regions, although the array provides no information on how far to the north these waters are carried beyond 34.5°S. Similarly, the time-mean flow that can clearly be tagged as AABW at this section is headed *southward* toward the formation region. The NADW recirculation is not too surprising, as DWBC recirculations in the NADW layer have been commonly observed at many locations along the DWBC pathway through the Atlantic (e.g., Schott et al. 2005; Johns et al. 2008; Meinen et al. 2012; Hummels et al. 2015). The AABW flow to the south, on the other hand, is somewhat unexpected, as it is counter to both previous hydrographic observations (e.g., Hogg et al. 1999; Mémery et al. 2000) and simple intuition given the location of the formation regions for the AABW.

Ocean Sci. Discuss., doi:10.5194/os-2016-76, 2016
Manuscript under review for journal Ocean Sci.
Published: 17 October 2016

325 The historical observations of the flow in this region have primarily been geostrophic
326 estimates relative to an assumed level of no motion, which absolute velocity observations
327 here and elsewhere in the DWBC have called into question (e.g., Meinen et al. 2012;
328 Meinen et al. 2013a). The few absolute observations that have been obtained previously
329 in the region, Lagrangian float and direct current meter measurements around 28-30ºS in
330 the Brazil Basin, also found hints of recirculation in both the NADW and AABW layers
331 (e.g., Hogg and Owens 1999; Hogg et al. 1999). There is no question, however, that
332 AABW is observed further north, reaching at least the subtropical North Atlantic in the
333 western half of the Atlantic basin (e.g., Frajka-Williams et al. 2011). The hydrographic
334 observations reported by Coles et al. (1996) provide a possible answer to this conundrum,
335 suggesting a possible interior pathway that would bring AABW to the Vema Channel
336 along the western flank of the Mid-Atlantic Ridge, which would be offshore of the PIES
337 array presented here. Another possible reason is simply that two years is insufficient to
338 identify the mean flow; the average velocity over the full five year record between Sites
339 C and D in the AABW layer is very weakly northward (but not statistically significantly
340 different from zero). A detailed analysis of the water masses and their variability is
341 beyond the scope of the present study, and these issues will be revisited in a future
342 manuscript using hydrographic and lowered acoustic Doppler current profiler data that is
343 being collected on recent and near-future cruises. The results shown here do, however,
344 highlight the importance of collecting and interpreting absolute velocities near the
345 boundary, and not just relative velocities.
346
347 *Observed deep flow variability*

Ocean Sci. Discuss., doi:10.5194/os-2016-76, 2016
Manuscript under review for journal Ocean Sci.
Published: 17 October 2016

As has been noted at several other latitudes along the pathway of the DWBC, the temporal variability of the DWBC flow greatly exceeds the time-mean values (e.g. Schott et al. 2004, 2005; Toole et al. 2011; Johns et al. 2008; Send et al. 2011; Hummels et al. 2015). The deep flow variability at 34.5°S is no exception (Figure 5). Many/most of the strongest variations in the deep flow within the NADW layer (2000-3200 dbar; right panel in Figure 5) are also observed in the mid-depth and surface layers (center and left panels in Figure 5, respectively). The shear between layers is not constant, however, with some events having similar transport in the NADW layer and the mid-depth layer above (see June 2009 anomalously northward flow event in the middle and offshore parts of the array in Figure 5, center and right panels), while others can be much more intense in one layer than the other (see the anomalously northward flow in the May-June 2012 event and the February-March 2014 event in the offshore parts of the array in Figure 5 where the transport signal in the NADW layer is much larger than in the mid-depth layer immediately above). Interestingly, these intense events in the deep layer are sufficiently large at times that the cumulative NADW flow integrated offshore will reverse sign (see white contours in the right panel of Figure 5), indicating that the offshore recirculation to the north at times exceeds the southward flow of the DWBC itself. In most cases the deep flow, i.e. the flow deeper than 800 dbar, is highly correlated in terms of variability. For example, the transport integrated across the array from Site A to Site D within vertical limits of *either* 800-to-4800 dbar or 2000-to-3200 dbar yields time series that are very highly correlated[3] within one another (r = 0.98). For the remainder of the paper,

[3] Some might suspect this high correlation could be artificial due to the calculation of transport via the single 'gravest' mode inherent in the PIES/CPIES analysis technique. While a single 'mode' is used in this manner, a similar correlation analysis of the deep transport integrated in the OFES model yields a very similar high value (r = 0.95).

Ocean Sci. Discuss., doi:10.5194/os-2016-76, 2016
Manuscript under review for journal Ocean Sci.
Published: 17 October 2016

369 unless otherwise noted the deep transports will be integrated between 800 and 4800 dbar
370 (or the seafloor where shallower).
371
372 Integrating the meridional transport through the largest possible DWBC layer, from 800
373 dbar down to 4800 dbar and across the entire array between Sites A and D, it becomes
374 clear that these strong events can reverse the deep flow for periods of a few days to a few
375 months (Figure 6, black solid line; see also Table 2)[4]. The resulting time-mean value (-
376 15.2 Sv) is a bit smaller than would be expected given previous moored observations
377 upstream at 11°S (-16.9 Sv for the NADW layer only, Schott et al. 2005; -17.5 Sv for the
378 DWBC, Hummels et al. 2015). It is also a bit smaller than the averages estimated from
379 repeated ship sections at 5°S (e.g. -17.3 Sv; Schott et al. 2005, estimated roughly between
380 800-4800 dbar from their Figure 7a) and at 11°S (e.g. -22.5 Sv; Schott et al. 2005,
381 estimated roughly between 800-4800 dbar from their Figure 7b). This lower transport at
382 34.5°S would be consistent with the Garzoli et al. (2015) pathway analysis that suggests
383 that ~20% of the DWBC transits off toward the eastern side of the basin at around 20°S;
384 note that the Garzoli et al. study used the same OFES model run as one of its analysis
385 data sets, so the results are not fully independent from the results presented here. The
386 PIES mean DWBC transport value at 34.5°S is roughly comparable with the widely
387 varying previous estimates of the MOC at this latitude (e.g. -12.4 Sv from an inverse

[4] Note that the transport integrated over the full record (2009-2014) within the 800-4800 dbar level from Site A to Site D does not use the data from Sites AA and BB, as those two sites are only available during 2012-2014. Because of the sloping topography, the transports integrated with or without Sites AA and BB are slightly different, due to the well-known 'bottom triangle' issue, however the differences are very small. For the period when all sites are available, the transports calculated either with or without Sites AA and BB are correlated with each other with a value of r = 0.97, with a mean difference of 1.4 Sv and a standard deviation of the differences of 5.2 Sv (the standard deviation drops to about 3.8 Sv after a 30-day lowpass filter). The variance associated with the differences between the two transport time series (26.9 Sv^2) represents about 5% of the actual variance in the time series (537.8 Sv^2 without Sites AA and BB; 516.4 Sv^2 with Sites AA and BB).

Ocean Sci. Discuss., doi:10.5194/os-2016-76, 2016
Manuscript under review for journal Ocean Sci.
Published: 17 October 2016

388 estimate using hydrographic sections at 32°S, Lumpkin and Speer 2007; -18.1 Sv from
389 repeated expendable bathythermograph sections, Garzoli et al. 2013), as it should be if
390 the bulk of the lower limb of the MOC is carried by the DWBC. However, it must be
391 noted that due to the leveling issue discussed earlier, the time mean calculated herein for
392 the DWBC at 34.5°S is partially dependent on the OFES model velocity at 1500 dbar as
393 noted earlier. As such, the time-mean is not the focus here.
394
395 The DWBC variability is demonstrated clearly by the large standard deviation (22.8 Sv)
396 and the wide peak-to-peak range (139.4 Sv). Even after smoothing with a 30-day low-
397 pass filter, the standard deviation is large (20.8 Sv) and the peak-to-peak range exceeds
398 95 Sv. These variations are somewhat larger than the ~80 Sv peak-to-peak range
399 observed at 11°S (e.g. Schott et al. 2005; Hummels et al. 2015), however this likely
400 reflects a larger integration domain used at 34.5°S where the array stretches further
401 offshore (~650 km vs. 250 km) and captures more of the DWBC recirculation. As will
402 be shown shortly, integrating the transport at 34.5°S to a roughly similar 200 km distance
403 offshore yields smaller peak-to-peak transport of ~60 Sv, which is more comparable with
404 the previous values observed at 11°S.
405
406 The mechanisms behind these large variations will be addressed later in the paper, but
407 before continuing to that topic it is instructive to further characterize the nature of the
408 variations themselves. The transport can be broken into a component relative to an
409 assumed reference level of no motion (e.g. the 'baroclinic', or vertically sheared,
410 component, Figure 6, blue dashed line) and a component associated with the actual

Ocean Sci. Discuss., doi:10.5194/os-2016-76, 2016
Manuscript under review for journal Ocean Sci.
Published: 17 October 2016

411 reference level velocity (e.g. the 'barotropic', or vertically constant, component, Figure 6,
412 red dash-dot line). The former is calculated here relative to an assumed zero flow at 800
413 dbar, while the latter is simply the true reference level (800 dbar) velocity multiplied by
414 the DWBC integration area. It immediately becomes evident that the transport relative to
415 an assumed level of no motion at 800 dbar (Figure 6, blue dashed line) bears little
416 relationship to the true absolute transport in the DWBC layer (Figure 6, black solid line).
417 The relative contribution to the absolute flow is much smaller than the reference layer
418 contribution, and the two components are statistically uncorrelated with one another (r = -
419 0.28). The absolute transport is highly correlated with the reference transport (r = 0.91),
420 and is not significantly correlated with the relative transport (r = 0.14), however that is
421 not to say that the relative contribution is unimportant. While the relative term is
422 typically 10 Sv or less, in some events it greatly exceeds this value, with one event in late
423 2009 having a southward relative component exceeding 40 Sv in amplitude for more than
424 a month. In addition to illustrating the fact that the 'baroclinic' term and the 'barotropic'
425 term are uncorrelated, consistent with what has been observed at this location with the
426 first year of data along 34.5°S (Meinen et al. 2012) and at other latitudes (e.g. 26.5°N;
427 Meinen et al. 2013a), these results make clear that both the 'baroclinic' and the
428 'barotropic' terms must be measured directly to quantify the DWBC flow.
429
430 *Spectral distribution of observed DWBC energy*
431 When the first year of data at 34.5°S was published (Meinen et al. 2012), it was not
432 possible to evaluate whether there was an annual cycle in the DWBC transport, although
433 analysis of the OFES model at that time suggested that there was a very weak, albeit not

Ocean Sci. Discuss., doi:10.5194/os-2016-76, 2016
Manuscript under review for journal Ocean Sci.
Published: 17 October 2016

434 significant, seasonal signal. With nearly five years of real data now available, this can be
435 revisited (Figure 7). With the additional years there is still no obvious annual cycle in the
436 data, even after applying a 30-day low-pass filter to eliminate the higher-frequency
437 signals. The average annual cycle (red line in Figure 7) perhaps hints at a northward
438 anomaly in the first half of the year and a southward anomaly in the second half of the
439 year, consistent with the earlier analysis of the OFES model (Meinen et al. 2012). This
440 observed annual signal is very weak and is highly influenced by other time scales and
441 aliasing. Interestingly, at 26.5°N the pattern is initially the same, as there is no
442 meaningful annual cycle in the DWBC integrated out to ~500 km from the boundary
443 (Meinen et al. 2013a). At 26.5°N, if the DWBC is integrated over a narrower domain
444 spanning only the 'mean' location of the DWBC and not including the recirculations
445 offshore, then an annual cycle is apparent. Following the same idea here for 34.5°S, the
446 annual cycle was explored for the deep transport integrated only between Sites A and B,
447 which spans the 'mean' location of the DWBC at this latitude (see Figure 2). Unlike at
448 26.5°N, there is still no clear annual cycle at 34.5°S even when integrated across this
449 narrower span, and the amplitudes are a factor of 2-4 smaller (not shown). Whether this
450 is a dynamical difference between the two latitudes or merely a sign that additional years
451 of data are needed to tease out the annual cycle at 34.5°S is an area for future research.
452 However, it should be noted that the continuous DWBC record integrated similarly at
453 11°S shows no obvious stable annual cycle either (e.g. Dengler et al. 2004; Schott et al.
454 2005).
455

Ocean Sci. Discuss., doi:10.5194/os-2016-76, 2016
Manuscript under review for journal Ocean Sci.
Published: 17 October 2016

Spectral analysis of the continuous portion (2011-2014) of the absolute transport time series (integrated from Site A to Site D) finds little energy at either the semi-annual or annual periods, with the largest signature being a broad peak spanning periods of 90-160 days centered near 145 days (Figure 8). The relatively short record compared to this time scale results in fairly wide error bars for the spectrum, so the spectral distribution may yield more nuanced results once a few more years of data have been collected. There are noisy spectral peaks in the 20-50 day band. Previous observations focusing on the upper ocean just south of the SAM array (near 37° to 38°S) by Garzoli and Simionato (1990) found wave signals in this same frequency band, which were attributed to both eastward propagating Topographic Rossby Waves (TRWs) and to westward propagating frontal perturbations. The latter are likely to be quite different at 34.5°S, which is well outside of the more energetic Confluence region, however the TRWs are quite likely to be present in the region around 34.5°S. Further discussion of the sources of the observed DWBC variations will be presented shortly. Breaking the observed variance into temporal bands (Table 3), the Site A to Site D transport signal clearly has little energy at the semi-annual or annual periods, each representing less than 3% of the total variance. The bulk of the energy in the transport time series is at time scales shorter than 170 days. There is a modest amount of energy at time scales between semi-annual and annual, and nearly 15% of the energy is at periods longer than annual in the observed record. Because the record used for the spectral analysis is only a bit over three years long, the analysis of the data likely underestimates the energy available at periods longer than annual. The breakdown by period bands is generally similar when calculated for transports integrated only between Sites A and B (Table 3, parentheses), however the

Ocean Sci. Discuss., doi:10.5194/os-2016-76, 2016
Manuscript under review for journal Ocean Sci.
Published: 17 October 2016

annual and semiannual energy is a bit higher when integrated within that narrow band, despite there being no obvious visual annual cycle.

Characterizing the deep flow variations

Characterizing the nature of these flow variations could be approached via Empirical Orthogonal Function analysis (e.g. Emery and Thomson 1997), however the resulting eigenvalues are not statistically significant from one another – i.e. they are 'degenerate' (North et al. 1982) and cannot be physically interpreted in a meaningful way, which may be at least partially due to the relatively short record length. Instead, to characterize the vertical-horizontal structure of these transport variations, composite averages were created based on the transport integrated from 800 to 4800 dbar (or the bottom where shallower) and from Site A to Site D (i.e. the black line in Figure 6). Composite mean sections of meridional velocity were created for 'strong' days, where the southward transport, integrated within the above-described bounds, was greater than the record-length time-mean plus two statistical standard errors of the mean (the standard error was estimated to be 5.2 Sv based on the estimated integral time scale of 17 days; see solid and dashed gray lines in Figure 6), for 'weak days' where the southward transport was less than the record-length time-mean minus two statistical standard errors of the mean, and for 'middle' days with transports within ± two statistical standard errors around the time-mean (Figure 9). Only the time period where the additional instruments at Sites AA and BB were available was used in creating the composites as this provides the best horizontal resolution of data.

Ocean Sci. Discuss., doi:10.5194/os-2016-76, 2016
Manuscript under review for journal Ocean Sci.
Published: 17 October 2016

502 The resulting composites suggest that the anomalous flows have a certain 'barotropicity'
503 inshore of around 49°W, with stronger southward DWBC flows below 1000 dbar
504 corresponding to stronger southward Brazil Current flows above 1000 dbar on 'strong'
505 days, and weaker southward flow in shallow and deep layers on 'weak' days (Figure 9).
506 There is also a hint of an offshore shift of the deep flow on weak days. The zero crossing
507 locations (white contours in Figure 9) seem to be fairly constant in the upper layer, while
508 below roughly 2000 dbar this is not true. By contrast to the apparent 'barotropicity' of
509 the flows near to the continental slope, offshore of around 49°W the composite results
510 suggest significant 'baroclinicity' (i.e. increased vertical shear), with weak northward
511 flow (or even southward flow) at depth but intensified northward flow near the surface on
512 'strong' days, but reduced 'baroclinicity' (i.e. reduced shear) on the 'weak' days. Recall
513 that the definition for 'strong' and 'weak' here is based on the integral of the deep flow
514 across the entire section, so in phase flow anomalies in the deep layer are perhaps an
515 artifact of how the composites are created. Correlation of the deep flows between pairs
516 of PIES/CPIES is quite low, so blending the inshore and offshore deep flows may not
517 provide the clearest separation of events, although integrating the deep flow across the
518 array should in theory provide the best estimate of the 'throughput' of the DWBC by
519 attempting to average out the recirculation offshore. As has been noted in the North
520 Atlantic at 26.5°N however, these recirculations may reach all the way to the Mid-
521 Atlantic Ridge (Meinen et al. 2013a), which if also true at 34.5°S would suggest that
522 some of the recirculation is beyond the range of the array (note that at 34.5°S the Mid-
523 Atlantic Ridge is about 2500 km east of site D).
524

Ocean Sci. Discuss., doi:10.5194/os-2016-76, 2016
Manuscript under review for journal Ocean Sci.
Published: 17 October 2016

525 To test whether composites based solely on the DWBC flow (and not the recirculation)
526 might produce a clearer picture with regards to the deep inshore and offshore meridional
527 flows, an alternate definition for 'strong' and 'weak' was developed based only on the
528 deep transport integrated between Sites A and B (Figure 10). The standard deviation of
529 the deep transport variability integrated between Sites A and B is less than half that of the
530 deep transport integrated across the entire array (Table 4), but the peak-to-peak range still
531 exceeds 50 Sv within the narrower span. The statistical standard error of the mean is 1.1
532 Sv, and the integral time scale is about 6 days, suggesting that higher frequencies play a
533 larger role in the observed variability in the narrower span between Sites A and B. The
534 'strong' and 'weak' days in the record were again defined as days where the meridional
535 transport experienced southward or northward anomalies greater than two statistical
536 standard errors, respectively. The resulting composites (Figure 11) show similarities to
537 the earlier versions (Figure 9) inshore of about 49°W, with the anomalous flow having
538 significant 'barotropicity'. The near-slope anomalies are even stronger in these
539 composites, with noticeably stronger flows at all depths on the 'strong' days (compare the
540 lower right panels of Figures 9 and 11), and much weaker flows at all depths on the
541 'weak' days (compare the top right panels of Figures 9 and 11). Offshore of 49°W, the
542 composites are quite different from those determined using the Site A to Site D
543 definition. The composites based on the Site A to Site B definition show more
544 'barotropicity' offshore of 49°W, whereas the earlier composites showed more
545 'baroclinicity' (i.e. enhanced shear), particularly on 'strong' days. This dichotomy
546 between the two sets of composites suggests two facts about the deep flows: a) the deep
547 near-slope flows are often in phase with the upper layer flows; and b) the deep near-slope

Ocean Sci. Discuss., doi:10.5194/os-2016-76, 2016
Manuscript under review for journal Ocean Sci.
Published: 17 October 2016

548 flows are often 180° out-of-phase with the deep flows immediately offshore (e.g. when
549 the deep southward flow between the slope and 49°W intensifies, the recirculation to the
550 north between 49°W and 47°W also intensifies). Note that this pattern is also observed in
551 the upper layer, where strong northward recirculations are associated with strong Brazil
552 Current events (Figure 11d).
553
554 This apparent anti-correlation between the deep flow near the slope and the recirculation
555 offshore is somewhat surprising, since as was noted earlier, there is only a very weak
556 correlation between the flow between pairs of PIES. The correlation values between the
557 deep flows integrated in the Site A to Site B span and the deep flows integrated in the
558 Site B to Site C span is about r = -0.4. Based on the average integral time scale for these
559 two records (8 days) and the record length, this correlation value is statistically
560 significantly different from zero at even the 99% level (cutoff r = |0.38|), but a linear
561 relationship between the two would explain less than 20% of the observed variability.
562 Lagged-correlations show insignificant values with a shift of more than a few days in
563 either direction, and this is true for not only the daily records but also for records that
564 have been low-pass filtered (2^{nd} order Butterworth passed both forward and back) with
565 cutoff periods of 10, 30, and 90 days. So while the composites suggest that on average
566 the recirculation offshore intensifies when the southward DWBC flow increases, and vice
567 versa, the actual flow at any given time is more complex and nuanced. Clearly the deep
568 flow in this region is influenced by many different factors, but the observational array,
569 while well suited to capture the deep meridional transport variability near the western
570 boundary, has limited ability to track deep flow features migrating into the region.

Ocean Sci. Discuss., doi:10.5194/os-2016-76, 2016
Manuscript under review for journal Ocean Sci.
Published: 17 October 2016

571 Therefore, an evaluation in a numerical model may aid in the interpretation of the
572 observed signals and help extract more information (as was also done in the earlier
573 Meinen et al. 2012 study).
574
575 *Modeled deep flow variability*
576 Integrating the meridional velocity from the OFES model within the same longitude
577 range (between Sites A and D) and over the same pressure range (800 to 4800 dbar or the
578 bottom where it is shallower) using the 27-years of model output yields a robust DWBC
579 with a time-mean similar to the observed value (Figure 12, see also Table 5). While the
580 time-mean values are similar (recall that the model 1500 dbar mean value is imposed on
581 the data, and therefore the means are not completely independent), the time variability
582 from the model is somewhat smaller than that of the real ocean (standard deviation of
583 16.5 Sv versus 22.8 Sv, respectively). As in the real ocean, there is little sign of an
584 annual cycle in the model DWBC transport – perhaps a hint of anomalous northward
585 flow in the first half of the year (Figure 12, lower panel), and anomalous southward flow
586 in the second half, but the variability at other time scales clearly dominates. The
587 percentage of variance explained by the annual or semi-annual periods is less than 10%
588 each (Table 6), although the annual and semi-annual percentage values are a factor of 2-3
589 larger than the comparable values for the observed time series (Table 3). Because the
590 model output record is much longer than the real data set, it is possible to evaluate how
591 much energy is in the longer periods; evaluation both in period bands (Table 6) and as a
592 spectrum (Figure 13) illustrates that the DWBC in the model does not have much energy
593 at periods longer than two years. Even using extended windows for calculating the

Ocean Sci. Discuss., doi:10.5194/os-2016-76, 2016
Manuscript under review for journal Ocean Sci.
Published: 17 October 2016

spectra does not extract much energy at the longer time scales (compare Figure 13 panels b, c, and d). What is clear is that the model variability is weaker than that in the actual observations at essentially all time scales (compare Figure 13a to panels b-d). Nevertheless, the model does show a broad peak of energy centered around 140-160 days, just as the observations show, so it is clear that in general the model DWBC has similar, if perhaps too weak, variability when compared to that of the real ocean.

Having verified that the DWBC variability in the model is qualitatively similar to that in the real ocean (for periods shorter than two years), it is reasonable to then 'step back' and evaluate a larger domain within the model to try and identify the sources/mechanisms behind the variations observed near the continental slope. As a first step toward this goal, a Hovmoller plot of the OFES meridional velocity at the central depth of the NADW near 2600 m across 34.5°S between the western continental slope and the Mid-Atlantic Ridge illustrates the presence of waves/eddies propagating both eastward and westward to the west of 40°W (Figure 14). The eastward trending features have propagation speeds of roughly 5-8 cm/s (4.5-7.0 km/day), while the westward trending features west of 40°W have propagation speeds of roughly 3-4 cm/s (2.5-3.5 km/day). East of about 40°W, the flow in the model is dominated by relatively weak features that propagate westward at a much slower speed – roughly 1 cm/s (0.9 km/day). These weaker features do not seem to propagate to the western portion of the basin, although it may be that they are simply obscured by the more energetic, faster features found nearer the continental slope. The propagation speeds for the region west of 40°W are in rough agreement with those found in an earlier inverted echo sounder (IES) array located just south of the PIES/CPIES array

Ocean Sci. Discuss., doi:10.5194/os-2016-76, 2016
Manuscript under review for journal Ocean Sci.
Published: 17 October 2016

discussed herein (Garzoli and Simionato 1990). This earlier study found that the eastward propagating signals had the characteristics of TRWs, and given the similar or perhaps even slightly steeper topography in the study region discussed in this study, such a diagnosis seems equally likely here.

The westward propagating features in the model are consistent with Rossby Wave-like features that have been identified at other latitudes (e.g. Meinen and Garzoli 2014), with propagation speeds that are slightly faster than linear first-mode baroclinic Rossby Wave theory would predict, which is consistent with historical satellite altimeter observations (e.g. Chelton and Schlax 1996; Polito and Liu 2003, Osychny and Cornillon 2004) as well as some recent theoretical work (e.g. Paldor et al. 2007; De Leon and Paldor 2009). Note that some studies point out that these features are in fact more likely "coherent vortices" rather than Rossby Waves, since they are closed circulation features that can translate properties, which waves cannot do (e.g. Chelton et al. 2007). More recently, Polito and Sato (2014) have shown that the dynamics may in fact be a bit more nuanced, presenting evidence that these eddies tend to 'ride' on Rossby Waves.

The closed nature of these westward propagating features is clear in the model when the model output is viewed as monthly averages. Perhaps the most prominent westward propagating feature in this model run occurs in the latter half of 1987, with a strong clear southward velocity anomaly propagating westward from about 44°W to the boundary (Figure 14). Evaluating monthly averages of the deep model velocity at 2600 m depth (i.e. near the core depth for the NADW component of the DWBC) during the last five

Ocean Sci. Discuss., doi:10.5194/os-2016-76, 2016
Manuscript under review for journal Ocean Sci.
Published: 17 October 2016

640 months of 1987 and comparing them to the long-term mean velocity easily highlights a
641 closed circulation feature that causes this westward propagating southward velocity
642 anomaly (Figure 15).
643
644 The long-term mean from the model (Figure 15a) clearly shows the southward DWBC
645 hugging the continental slope at the latitude of the PIES/CPIES array (yellow line), while
646 in the long-term mean field there is only quite weak circulation in comparison in the
647 offshore portions of the array. The monthly averages from the model for the final five
648 months of 1987 (Figure 15b-f), however, illustrate the highly energetic flows that can be
649 found offshore at any particular time. A strong anticyclonic feature, highlighted by the
650 magenta disc in Figure 15, slowly propagates westward from August through December
651 1987. The radius of the disc of anticyclonic flow, which was subjectively determined
652 based on the mapped velocities, is roughly 180-200 km for most of the months shown
653 (except for December, Figure 15f, when it drops to around 120 km). The baroclinic
654 Rossby Radius (NH/f, where the Brunt-Väisälä frequency $N = 0.0018\ s^{-1}$ is a typical mid-
655 depth value, the water depth $H = 4500$ m, and f is the Coriolis parameter) in this area is
656 roughly 100 km, so about a factor of two smaller than the observed anticyclonic feature.
657 (N.B. – The barotropic Rossby Radius, given by $(gH)^{½}/f$, where g is gravity, is much
658 larger, around 2500 km at this latitude.) As such, referring to these propagating features
659 as 'coherent vortices' is perhaps more appropriate, but some of the features may represent
660 long Rossby Waves (Polito and Sato 2015). Regardless, it is clear that these large
661 westward propagating features are creating the largest transport anomalies in the deep

Ocean Sci. Discuss., doi:10.5194/os-2016-76, 2016
Manuscript under review for journal Ocean Sci.
Published: 17 October 2016

662 layers in the model, and the correspondence between model and observations where it
663 can be tested suggests that this is likely true in the real ocean as well.
664
665 **Conclusions:**
666 As has been found at other locations along the DWBC path through the Atlantic, at
667 34.5°S the time-varying intensity of the DWBC volume transport during 2009-2014 (22.8
668 Sv standard deviation) greatly exceeds the time-mean value (-15.2 Sv) – which illustrates
669 the necessity of continuous observation to avoid aliasing. The spectral character of the
670 observed variability has a broad peak within roughly 90-160 days, centered near 145
671 days, with additional energy found in the 20-50 day band. Composite analysis
672 (integrated between both Site A to D and Site A to B) suggests that the variations near the
673 continental slope west of 49°W have some 'barotropicity', in the sense that they affect
674 the flow at all layers including near the sea surface. The composite results also show that
675 the strong southward transport anomalies near the slope are partially compensated by
676 increased recirculation to the north immediately offshore of 49°W, while weak southward
677 transport anomalies near the slope are also partially compensated by decreased
678 recirculation to the north offshore of 49°W.
679
680 Coupled with analysis of the time-varying flow along the array and analysis of the
681 broader area in a high-quality, high resolution, well-validated numerical model, the
682 results suggest that the dominant source of transport variations near the continental slope
683 are westward propagating coherent vortices that superimpose on top of and modulate the
684 intensity of the DWBC flow to yield large southward or northward anomalies depending

Ocean Sci. Discuss., doi:10.5194/os-2016-76, 2016
Manuscript under review for journal Ocean Sci.
Published: 17 October 2016

685 on the flow associated with the vortices. This suggests that the observing array might be
686 enhanced/improved through the addition of either/both increased horizontal resolution of
687 observations (to more clearly identify these propagating features) and/or the expansion of
688 the array out toward the Mid-Atlantic Ridge (to more completely capture the offshore
689 recirculations). The results also demonstrate the necessity of directly and independently
690 capturing both the 'baroclinic' (vertically sheared) and 'barotropic' (vertically coherent)
691 flows in order to properly understand the absolute transport variability of the DWBC at
692 this location.

693

694

695 **Acknowledgements:**

696 The authors would like to thank the ship captains and crews of the N.H. Cruzeiro do Sul,
697 A.R.A. Puerto Deseado, S.V. Ice Lady Patagonia II, N.Oc. Alpha-Crucis, and the N.Oc.
698 Alpha Delphini, who have all ably supported our research cruises in support of this
699 project. Ulises Rivero, Rigoberto Garcia, Pedro Pena, Carlos Franca, Marcela Charo,
700 Daniel Valla and the support teams in Miami, Sao Paulo and Buenos Aires all have
701 helped collect and process the data presented herein. The U.S. PIES/CPIES observations
702 and the participation of CM, SG, RP, and SD were supported via the NOAA Climate
703 Program Office-Climate Observations Division (FundRef number 100007298) under the
704 Southwest Atlantic Meridional Overturning Circulation ("SAM") project, with additional
705 support from the NOAA Atlantic Oceanographic and Meteorological Laboratory. SG
706 and RP were also supported in part under the auspices of the Cooperative Institute for
707 Marine and Atmospheric Studies (CIMAS), a Cooperative Institute of the University of
708 Miami and NOAA, cooperative agreement NA10OAR4320143. RP acknowledges
709 additional support from NOAA (Grant NA13OAR4310131) and NASA (Grant
710 NNX14AH60G). The Brazilian CPIES observations were supported by the São Paulo
711 State Research Foundation (FAPESP) through the SAMOC-Br project (Grant
712 2011/50552-4). EC acknowledges CNPq for a Research Fellowship (Grant 302018/2014-
713 0). Hydrographic observations were partially supported by the Inter-American Institute
714 for Global Change Research (IAI) grants SGP2076 and CRN3070. The IAI is supported
715 by the US National Science Foundation (grants GEO-0452325 and GEO-1128040). The
716 merged, multi-sensor L4 Foundation sea-surface temperature (SST) data used herein
717 were provided by the NASA Jet Propulsion Laboratory under support from the NASA
718 MEaSUREs program. Rick Lumpkin and Arthur Mariano provided several helpful ideas

Ocean Sci. Discuss., doi:10.5194/os-2016-76, 2016
Manuscript under review for journal Ocean Sci.
Published: 17 October 2016

719 while the manuscript was being prepared, and Libby Johns gave a number of suggestions
720 for improving an earlier draft of the paper.
721

722

Ocean Sci. Discuss., doi:10.5194/os-2016-76, 2016
Manuscript under review for journal Ocean Sci.
Published: 17 October 2016

723 **References:**
724
725 Ansorge I., M. Baringer, E. Campos, S. Dong, R. A. Fine, S. Garzoli , G. Goni, C.
726 Meinen, R. Perez, A. Piola, M. Roberts, S. Speich, J. Sprintall, T. Terre, and M. van den
727 Berg, Basin-Wide Oceanographic Array Bridges the South Atlantic, *EOS Transactions*,
728 AGU, 95(6), 53-54, 10.1002/2014EO060001, 2014.
729
730 Arhan, M., H. Mercier, and Y.-H. Park, On the deep water circulation of the eastern
731 South Atlantic Ocean, *Deep Sea Res. I*, 50, 889-916, doi:10.1016/S0967-0637(03)00072-
732 4, 2003.
733
734 Bryden, H. L., B. A. King, and G. D. McCarthy, South Atlantic overturning circulation at
735 24°S, *J. Mar. Res.*, 69, 39-56, doi:10.1357/002224011798147633, 2011.
736
737 Buckley, M. W., and J. Marshall, Observations, inferences, and mechanisms of the
738 Atlantic Meridional Overturning Circulation: A review, *Rev. Geophys.*, 54, 5-63,
739 doi:10.1002/2015RG000493, 2016.
740
741 Chelton, D. B., and M. G. Schlax, Global observations of oceanic Rossby Waves,
742 *Science*, 271, 234-238, 1996.
743
744 Chelton, D. B., M. G. Schlax, R. M. Samelson, and R. A. de Szoeke, Global observations
745 of large oceanic eddies, *Geophys. Res. Lett.*, 34, L15606, doi:10.1029/2007GL030812,
746 2007.
747
748 Chin, T. M., R. F. Milliff, and W. G. Large, Basin-Scale, High-Wavenumber Sea Surface
749 Wind Fields from a Multiresolution Analysis of Scatterometer Data, *J. Atmos. Ocean.*
750 *Tech.*, 15, 741–763, 1998.
751
752 Coles, V. J., M. S. McCartney, D. B. Olson, and W. M. Smethie Jr., Changes in Antarctic
753 Bottom Water properties in the western South Atlantic in the late 1980s, *J. Geophys.*
754 *Res.*, 101 (C4), 8957-8970, 1996.
755
756 Dengler, M., Schott, F. A., Eden, C., Brandt, P.,Fischer, J., and Zantopp, R., Break-up of
757 the Atlantic Deep Western Boundary Current into eddies at 8°S, *Nature*, 432, 1018–1020,
758 doi:10.1038/nature03134, 2004.
759
760 De Leon, Y., and N. Paldor, Linear waves in midlatitudes on the rotating spherical Earth,
761 39 (12), 3204-3215, doi:10.1175/2009JPO4083.1, 2009.
762
763 Dewar, W. K., and J. M. Bane, Subsurface Energetics of the Gulf Stream near the
764 Charleston Bump, *J. Phys., Oceanogr.*, 15 (12), 1771-1789, 1985.
765
766 Dijkstra, H. A., Characterization of the multiple equilibria regime in a global ocean
767 model, *Tellus, Ser. A*, 59, 695–705, 2007.
768

Ocean Sci. Discuss., doi:10.5194/os-2016-76, 2016
Manuscript under review for journal Ocean Sci.
Published: 17 October 2016

769 Dong, S., S. L. Garzoli, M. O. Baringer, C. S. Meinen, and G. J. Goni, The Atlantic
770 Meridional Overturning Circulation and its Northward Heat Transport in the South
771 Atlantic, *Geophys. Res. Lett.*, 36, L20606, doi:10.1029/2009GL039356, 2009.
772
773 Dong, S., S. L. Garzoli, and M. O. Baringer, The role of inter-ocean exchanges on
774 decadal variations of the northward heat transport in the South Atlantic, *J. Phys.*
775 *Oceanogr.*, 41, 1498–1511, 2011.
776
777 Dong, S. , M. O. Baringer , G. J. Goni , C. S. Meinen , and S. L. Garzoli**,** Seasonal
778 variations in the South Atlantic Meridional Overturning Circulation from observations
779 and numerical models, *Geophys. Res. Lett*., 41, 4611-4618, doi:10.1002/2014GL060428,
780 2014.
781
782 Dong, S., G. Goni , and F. Bringas, Temporal variability of the Meridional Overturning
783 Circulation in the South Atlantic between 20°S and 35°S, *Geophys. Res. Lett.,* 42, 7655 -
784 7662*,* doi:10.1002/2015GL065603, 2015.
785
786 Donohue, K. D., Watts, D. R., Tracey, K. L., Greene, A. D., and Kennelly, M., Mapping
787 circulation in the Kuroshio Extension with an array of current and pressure recording
788 inverted echo sounders, *J. Atmos. Oceanic Tech.*, 27, 507–527,
789 doi:10.1175/2009JTECHO686.1, 2010.
790
791 Drijfhout, S. S., S. L. Weber, and E. van der Swaluw, The stability of the MOC as
792 diagnosed from model projections for pre-industrial, present and future climates, *Clim.*
793 *Dyn.*, 37, 1575-1586, doi:10.1007/s00382-010-0930-z, 2011.
794
795 Emery, W. J., and R. E. Thomson, *Data Analysis Methods in Physical Oceanography*,
796 Pergamon, Oxford, U. K., 1997.
797
798 Frajka-Williams, E., S. A. Cunningham, H. L. Bryden, and B. A. King, Variability of
799 Antarctic Bottom Water at 24.5°N in the Atlantic, *J. Geophys. Res.*, 116, C11026,
800 doi:10.1029/2011JC007168, 2011.
801
802 Frajka-Williams, E., C. S. Meinen, W.E. Johns, D.A. Smeed, A. Duchez, A.J. Lawrence,
803 D.A. Cuthbertson, G.D. McCarthy, H.L. Bryden, M.O. Baringer, B.I. Moat, and D.
804 Rayner, Compensation between meridional flow components of the AMOC at 26°N,
805 *Ocean Sci.,* 12, 481-493, doi:10.5194/os-12-481-2016, 2016.
806
807 Ganachaud, A., and C. Wunsch, Large-Scale Ocean Heat and Freshwater Transports
808 during the World Ocean Circulation Experiment, *J. Clim.*, 16, 696-705, 2003.
809
810 Garzoli, S., and C. Simionato, Baroclinic instabilities and forced oscillations in the
811 Brazil/Malvinas confluence front, *Deep-Sea Res.*, 37 (6), 1053-1074, 1990.
812
813 Garzoli, S. L., Geostrophic velocity and transport variability in the Brazil-Malvinas
814 Confluence, *Deep-Sea Res. I*, 40(7), 1379-1403, 1993.

Garzoli, S.L., and M.O. Baringer, Meridional heat transport determined with expendable bathythermographs, Part II: South Atlantic transport, *Deep-Sea Res. I*, 54(8), 1402-1420, 2007.

Garzoli, S.L and R. Matano, The South Atlantic and the Atlantic Meridional Overturning Circulation, *Deep-Sea Res. II*, 58, 1837-1847, doi:10.1016/j.dsr2.2010.10.063, 2011.

Garzoli, S.,M.O. Baringer, S. Dong, R. Perez, and Q. Yao, South Atlantic meridional fluxes, *Deep-Sea Res. I,* 71, 21-32, doi:10.1016/j.dsr.2012.09.003, 2013.

Garzoli, S.L., S. Dong, R. Fine, C. Meinen, R.C. Perez, C. Schmid, E. van Sebille, and Q. Yao, The fate of the Deep Western Boundary Current in the South Atlantic, *Deep-Sea Res. I* , doi: 10.1016/j.dsr.2015.05.008, 2015.

Goni, G., S. Kamholz, S. Garzoli, and D. Olson, Dynamics of the Brazil-Malvinas Confluence based on inverted echo sounders and altimetry, *J. Geophys. Res.*, 101(C7), 16273-16289, 1996.

Goni, G. J., F. Bringas, and P. N. DiNezio, Observed low frequency variability of the Brazil Current front, *J. Geophys. Res.*, 116 (C10037), doi:10.1029/2011JC007198, 2011.

Gordon, A. L., and C. L. Greengrove, Geostrophic circulation of the Brazil-Falkland confluence, *Deep-Sea Res.*, 33(5), 573-585, 1986.

Hogg, N. G., and W. B. Owens, Direct measurement of the deep circulation within the Brazil Basin, *Deep Sea Res. II*, 46, 335-353, 1999.

Hogg, N. G., G. Siedler, and W. Zenk, Circulation and Variability at the Southern Boundary of the Brazil Basin, *J. Phys. Oceanogr.*, 29 (2), 145-157, 1999.

Hogg, N. G., and A. M. Thurnherr, A Zonal Pathway for NADW in the South Atlantic, *J. Oceanogr.*, 61(3), 493-507, doi:10.1007/s10872-005-0058-7, 2005.

Hummels, R., P. Brandt, M. Dengler, J. Fischer, M. Araujo, D. Veleda, and J. V. Durgadoo, Interannual to decadal changes in the western boundary circulation in the Atlantic at 11°S, *Geophys. Res. Lett.*, 42, 7615–7622, doi:10.1002/2015GL065254, 2015.

Johns, W.E., L. M. Beal, M. O. Baringer, J. R. Molina, S. A. Cunningham, T. Kanzow, and D. Rayner, Variability of Shallow and Deep Western Boundary Currents off the Bahamas during 2004–05: Results from the 26°N RAPID–MOC array, *J. Phys. Oceanogr.*, 38, 605–623, doi/10.1175/2007JPO3791.1, 2008.

Johns, W. E., M. O. Baringer, L. M. Beal, S. A. Cunningham, T. Kanzow, H. L. Bryden, J. J. M. Hirschi, J. Marotzke, C. S. Meinen, B. Shaw, and R. Curry, Continuous, Array-

Based Estimates of Atlantic Ocean Heat Transport at 26.5°N, *J. Clim.*, 24, 2429-2449, doi:10.1175/2010JCLI3997.1, 2011.

Latif, M., N. Keenlyside, and J. Bader, Tropical sea surface temperature, wind shear, and hurricane development, *Geophys. Res. Lett.*, 34, L01710, doi:10.1029/2006GL027969, 2007.

Lopez, H., S. Dong, S.-K. Lee, and G. Goni, Decadal Modulations of Interhemispheric Global Atmospheric Circulations and Monsoons by the South Atlantic Meridional Overturning Circulation, *J. Clim.*, 29(3), 1831-1851, doi:10.1175/JCLI-D-15-0491.1, 2016.

Lumpkin, R., and K. Speer, Large-scale vertical and horizontal circulation in the North Atlantic Ocean, *J. Phys. Oceanogr.*, 33, 1902-1920, doi:0.1175/1520-0485(2003)033<1902:LVAHCI>2.0.CO;2, 2003.

Lumpkin, R., and K. Speer, Global Ocean Meridional Overturning, *J. Phys. Oceanogr.*, 37, 2550-2562, doi:10.1175/JPO3130.1, 2007.

Lumpkin, R., and S. Garzoli, Interannual to decadal changes in the western South Atlantic's surface circulation, *J. Geophys. Res.*, 116, C01014, doi:10.1029/2010JC006285, 2011.

Majumder, S., C. Schmid, and G. Halliwell, An observations and model-based analysis of meridional transport in the South Atlantic, *J. Geophys. Res. Oceans*, 121, doi:10.1002/2016JC011693, 2016.

Masumoto, Y., H. Sasaki, T. Kagimoto, N. Komori, A. Ishida, Y. Sasai, T. Miyama, T. Motoi, H. Mitsudera, K. Takahashi, H. Sakuma, and T. Yamagata, A fifty-year Eddy resolving simulation of the world ocean – Preliminary outcomes of OFES (OGCM for the Earth simulator), *J. Earth Simulator*, 1, 3556, 2004.

Matano, R. P., On the separation of the Brazil Current from the coast, 1993, *J. Phys. Oceanogr.*, 23, 79-90, doi:10.1175/1520-0485(1993)023<0079:OTSOTB>2.0.CO;2, 1993.

McCarthy, G. D., I. D. Haigh, J. J. Hirschi, J. P. Grist, D. A. Smeed, Ocean impact on decadal Atlantic climate variability revealed by sea-level observations, *Nature,* 521, 508–510, doi:10.1038/nature14491, 2015a.

Meinen, C. S. and D. R. Watts, Calibrating Inverted Echo Sounders equipped with Pressure Sensors, *J. Atmos. Oceanic Technol.*, 15(6), 1339-1345, 1998.

Meinen, C. S. and Watts, D. R., Vertical structure and transport on a Transect across the North Atlantic Current near 42°N: Time series and mean, *J. Geophys. Res.*, 105, 21869–21892, 2000.

Ocean Sci. Discuss., doi:10.5194/os-2016-76, 2016
Manuscript under review for journal Ocean Sci.
Published: 17 October 2016

Meinen, C. S., Garzoli, S. L., Johns, W. E., and Baringer, M. O., Transport variability of the Deep Western Boundary Current and the Antilles Current off Abaco Island, Bahamas, *Deep-Sea Res. I*, 51, 1397–1415, 2004.

Meinen, C. S., Baringer, M. O., and Garzoli, S. L.: Variability in Deep Western Boundary Current transports: Preliminary results from 26.5°N in the Atlantic, *Geophys. Res. Lett.*, 33, L17610, doi:10.1029/2006GL026965, 2006.

Meinen, C. S., A. R. Piola, R. C. Perez, and S. L. Garzoli, Deep Western Boundary Current transport variability in the South Atlantic: Preliminary results from a pilot array at 34.5°S, *Ocean Sci.*, 8, 1041-1054, doi:10.5194/os-8-1041-2012, 2012.

Meinen, C.S., W.E. Johns, S.L. Garzoli, E. Van Sebille, D. Rayner, T. Kanzow, and M.O. Baringer, Variability of the Deep Western Boundary Current at 26.5°N during 2004-2009, *Deep-Sea Res. II*, 85, 154-168, doi:10.1016/j.dsr2.2012.07.036, 2013a.

Meinen, C, S ., S. Speich, R. C. Perez , S. Dong , A. R. Piola, S. L. Garzoli , M. O. Baringer, S. Gladyshev, and E. J. D. Campos, Temporal variability of the Meridional Overturning Circulation at 34.5°S: Results from two pilot boundary arrays in the South Atlantic, *J. Geophys. Res.-Oceans,* 118, 6461-6478, doi:10.1002/2013JC009228, 2013b.

Mémery, L., M. Arhan, X. A. Alvarez-Salgado, M.-J. Messias, H. Mercier, C. G. Castro, and A. F. Rios, The water masses along the western boundary of the south and equatorial Atlantic, *Prog. Oceanogr.*, 47, 69-98, 2000.

North, G. R., T. L. Bell, R. F. Cahalan, and F. J. Moeng, Sampling Errors in the Estimation of Empirical Orthogonal Functions, *Mon. Wea. Rev.*, 110, 699-706, 1982.

Olson, D. B., G. P. Podesta, R. H. Evans, and O. B. Brown, Temporal variations in the separation of Brazil and Malvinas Currents, *Deep-Sea Res.*, 35, 1971–1990, 1988.

Osychny, V., and P. Cornillon, Properties of Rossby Waves in the North Atlantic estimated from satellite data, *J. Phys. Oceanogr.*, 34 (1), 61-76, 2004.

Paldor, N., S. Rubin, and A. J. Mariano, A consistent theory for linear waves of the Shallow-Water equations on a rotating plane in midlatitudes, 37 (1), 115-128, doi:10.1175/JPO2986.1, 2007.

Perez, R. C., S. L. Garzoli, C. S. Meinen, and R. P. Matano, Geostrophic velocity measurement techniques for the meridional overturning circulation and meridional heat transport in the South Atlantic, *J. Atmos. Oceanic Technol.*, 28, 1504–1521, doi:10.1175/JTECH-D-11-00058.1, 2011.

Ocean Sci. Discuss., doi:10.5194/os-2016-76, 2016
Manuscript under review for journal Ocean Sci.
Published: 17 October 2016

950 Perez, R. C., M. O. Baringer, S. Dong, S. L. Garzoli, M. Goes, G. J. Goni, R. Lumpkin,
951 C. S. Meinen, R. Msadek, and U. Rivero, Measuring the Atlantic meridional overturning
952 circulation, *Mar. Tech. Soc. J.*, 49(2), 167-177, doi:10.4031/MTSJ.49.2.14, 2015.
953
954 Polito, P. S., and W. T. Liu, Global characterization of Rossby waves at several spectral
955 bands, *J. Geophys. Res.*, 108, 3018, doi:10.1029/2000JC000607, C1, 2003.
956
957 Polito, P. S., and O. T. Sato, Do eddies ride on Rossby waves?, *J. Geophys. Res.*, 120,
958 5417–5435, doi:10.1002/2015JC010737, 2015.
959
960 Preu, B., F. J. Hernández-Molina, R. Violante, A. R. Piola, C. M. Paterlini, T. Schwenk,
961 I. Voigt, S. Krastel, and V. Spiess, Morphosedimentary and hydrographic features of the
962 northern Argentine margin: The interplay between erosive, depositional and gravitational
963 processes and its conceptual implications, *Deep-Sea Res. I*, 75, 157-174,
964 doi:10.1016/j.dsr.2012.12.013, 2013.
965
966 Rossby, T., On monitoring depth variations of the main thermocline acoustically, *J.*
967 *Geophys. Res.*, 74, 5542–5546, 1969.
968
969 Saraceno, M., C. Provost, A. R. Piola, J. Bava, and A. Gagliardini, Brazil Malvinas
970 Frontal System as seen from 9 years of advanced very high resolution radiometer data, *J.*
971 *Geophys. Res.*, 109, C05027, doi:10.1029/2003JC002127, 2004.
972
973 Sasaki, H., M. Nonaka, Y. Sasai, H. Uehara, and H. Sakuma, An eddy-resolving hindcast
974 simulation of the quasiglobal ocean from 1950 to 2003 on the Earth simulator, in *High*
975 *Resolution Numerical Modelling of the Atmosphere and Ocean*, edited by K. Hamilton
976 and W. Ohfuchi, pp. 157–185, Springer, New York, 2008.
977
978 Schmid, C., Mean vertical and horizontal structure of the subtropical circulation in the
979 South Atlantic from three-dimensional observed velocity fields, *Deep Sea Res. I*, 91, 50-
980 71, doi:10.1016/j.dsr.2014.04.015, 2014.
981
982 Schott, F.A., R. Zantopp, L. Stramma, M. Dengler, J. Fischer, and M. Wibaux,
983 Circulation and deep-water export at the western exit of the Subpolar North Atlantic, *J.*
984 *Phys. Oceanogr.*, 34(4), 817–843, 2004.
985
986 Schott, F. A., Dengler, M., Zantopp, R., Stramma, L., Fischer, J., and Brandt, P., The
987 Shallow and deep western boundary circulation of the South Atlantic at 5–11°S, *J. Phys.*
988 *Oceanogr.*, 35, 2031–2053, doi:10.1175/JPO2813.1, 2005.
989
990 Send, U., M. Lankhorst, and T. Kanzow, Observation of decadal change in the Atlantic
991 Meridional Overturning Circulation using 10 years of continuous transport data,
992 *Geophys. Res. Lett.*, 38, L24606, doi:10.1029/2011GL049801, 2011.
993
994 Smith, W. H. F., and D. T. Sandwell, Global Sea Floor Topography from Satellite
995 Altimetry and Ship Depth Soundings, *Science*, 277 (5334), l956-1962, 1997.
996

Ocean Sci. Discuss., doi:10.5194/os-2016-76, 2016
Manuscript under review for journal Ocean Sci.
Published: 17 October 2016

997 Srokosz, M. A., and H. L. Bryden, Observing the Atlantic Meridional Overturning
998 Circulation yields a decade of inevitable surprises, *Science*, 348 (6241),
999 doi:10.1126/science.1255575, 2015.
1000
1001 Stouffer, R. J., J. Yin, and J. M. Gregory, Investigating the causes of the response of the
1002 thermohaline circulation to past and future climate changes, *J. Clim.*, 19(8), 1365–1387,
1003 2006.
1004
1005 Thompson, R. O. R. Y., Coherence Significance Levels, *J. Atmos. Sci.*, 36 (10), 2020-
1006 2021, 1979.
1007
1008 Toole, J. M., R. G. Curry, T. M. Joyce, M. McCartney, and B. Peña-Molino, Transport of
1009 the North Atlantic Deep Western Boundary Current about 39°N, 70°W: 2004–2008,
1010 *Deep Sea Res. II*, 58, 1768–1780, 2011.
1011
1012 Tracey, K. L. and Watts, D. R., On Gulf Steam meander characteristics near Cape
1013 Hatteras, *J. Geophys. Res.*, 91, 7587–7602, 1986.
1014
1015 Trenberth, K. E., J. M. Caron, and D. P. Stepaniak, The atmospheric energy budget and
1016 implications for surface fluxes and ocean heat transports, *Clim. Dyn*., 17, 259-276, 2001.
1017
1018 Van Sebille, E., Johns, W. E., and Beal, L. M., Does the vorticity flux from Agulhas rings
1019 control the zonal pathway of NADW across the South Atlantic?, *J. Geophys Res.*, 117,
1020 C05037, doi:10.1029/2011JC007684, 2012.
1021
1022 Vellinga, M., and R. A. Wood, Global climatic impacts of a collapse of the Atlantic
1023 thermohaline circulation, *Clim. Change*, 54(3), 251–267, 2002.
1024
1025 Watts, D. R., and Kontoyiannis, H., Deep-ocean bottom pressure measurement: Drift
1026 Removal and performance, *J. Atmos. Oceanic Technol.*, 7, 296–306, 1990.
1027
1028 Watts, D. R., and Rossby, H. T., Measuring dynamic heights with inverted echo
1029 sounders: Results from MODE, *J. Phys. Oceanogr.*, 7, 345–358, 1977.
1030
1031 Zangenberg N., and Siedler, G., The path of the North Atlantic Deep Water in the Brazil
1032 Basin, *J. Geophys Res.*, 103, 5419–5428, 1998.
1033
1034
1035
1036
1037
1038
1039
1040
1041
1042

Ocean Sci. Discuss., doi:10.5194/os-2016-76, 2016
Manuscript under review for journal Ocean Sci.
Published: 17 October 2016

Tables

Site name	Instrument Type	Nominal Longitude	Nominal Latitude	Nominal Depth	Date of First Deployment
A	PIES	51° 30.0' W	34° 30.0' S	1360 m	March 18, 2009
AA	CPIES	50° 31.2' W	34° 30.0' S	2885 m	December 11, 2012
B	PIES	49° 30.0' W	34° 30.0' S	3535 m	March 18, 2009
BB	CPIES	48° 30.5' W	34° 30.0' S	4140 m	December 12, 2012
C	PIES	47° 30.0' W	34° 30.0' S	4540 m	March 19, 2009
D	PIES	44° 30.0' W	34° 30.0' S	4757 m	March 20, 2009

Table 1: Nominal locations, depths, and initial deployment dates of the PIES and CPIES moorings discussed in this paper. Note: The first instrument at Site B was a CPIES, but it was replaced with a PIES in July 2011.

	Daily	30-day low-pass filter
Mean	-15.2 Sv	-15.2 Sv
Median	-17.4 Sv	-17.4 Sv
Standard Deviation	22.8 Sv	20.3 Sv
Maximum value	+50.1 Sv	+35.0 Sv
Minimum value	-89.3 Sv	-60.8 Sv

Table 2: Statistics for the volume transport calculated from the PIES and GEM data. The transports were integrated from Site A to Site D (see Table 1) and from 800 dbar down to 4800 dbar (or the bottom, where it is shallower). Statistics were calculated over the period 2009 to 2014 using only the original PIES moorings.

Ocean Sci. Discuss., doi:10.5194/os-2016-76, 2016
Manuscript under review for journal Ocean Sci.
Published: 17 October 2016

Period band (days)	Variance [Sv^2]	Percentage of total variance
2 to 50	103.3 (83.1)	28.4 (25.9)
50 to 170	153.4 (61.0)	42.1 (19.0)
170 to 190	7.7 (54.9)	2.1 (17.1)
190 to 350	39.3 (54.0)	10.8 (16.8)
350 to 390	7.5 (54.9)	2.1 (17.1)
390 to record length	53.0 (12.8)	14.5 (4.0)

Table 3: Distribution of variance in the indicated period bands in the DWBC transport calculated from the PIES/CPIES observations during the continuous 2011-2014 window. The observed DWBC transport was integrated between 800 and 4800 dbar and between the original PIES at Site A and Site D. Values for transport integrated only between the PIES at Site A and Site B are shown in parentheses.

Integration span	Site A to Site D		Site A to Site B	
Integration period	2009-2014	2012-2014	2009-2014	2012-2014
Mean	-15.2 Sv	-18.0 Sv	-17.4 Sv	-17.2 Sv
Median	-17.4 Sv	-19.8 Sv	-17.2 Sv	-16.9 Sv
Standard Deviation	22.8 Sv	23.0 Sv	8.1 Sv	8.3 Sv
Maximum value	+50.1 Sv	+50.1 Sv	+18.1 Sv	+4.7 Sv
Minimum value	-89.3 Sv	-68.9 Sv	-46.5 Sv	-46.5 Sv

Table 4: Statistics for the volume transport calculated from the PIES and GEM data across the whole array (columns 2 & 3) versus only within the span between Site A and Site B (columns 4 & 5). Note that column 2 is identical to column 2 in Table 2. The transports were integrated from between the indicated sites (see Table 1) and from 800 dbar down to 4800 dbar (or the bottom where it is shallower). Statistics are shown for both the period 2009 to 2014 (columns 2 & 4) and during the enhanced array period 2012-2014 (columns 3 & 5). The transports were calculated using only the original PIES moorings; the results in the enhanced period are very similar if the CPIES are also included, as is to be expected for geostrophic calculations.

Ocean Sci. Discuss., doi:10.5194/os-2016-76, 2016
Manuscript under review for journal Ocean Sci.
Published: 17 October 2016

Integration span	Data mean	Data STD	Model mean	Model STD
Site A to Site B	-17.4 Sv	8.1 Sv	-17.6 Sv	7.6 Sv
Site A to Site D	-15.2 Sv	22.8 Sv	-16.0 Sv	16.5 Sv

Table 5: Time-mean and temporal standard deviation (STD) of the volume transport integrated between 800 and 4800 dbar (or the bottom where shallower) and between the indicated PIES locations. The observation-based estimates (middle columns) were calculated over the 2009-2014 time period; the model-based estimates (right two columns) were calculated over the 27-year run described in the text.

Period band (days)	Variance [Sv^2]	Percentage of total variance
6 to 50	60.0	19.2
50 to 170	105.7	33.8
170 to 190	20.8	6.7
190 to 350	56.9	18.2
350 to 390	27.3	8.7
390 to 1000	28.1	9.0
1000 to record length	13.6	4.3

Table 6: Distribution of variance in the indicated period bands in the DWBC transport calculated from the OFES model output. The model DWBC transport was integrated between 800 and 4800 dbar and between the longitudes of the real locations for the PIES at Site A and Site D.

Ocean Sci. Discuss., doi:10.5194/os-2016-76, 2016
Manuscript under review for journal Ocean Sci.
Published: 17 October 2016

1118 **Figures:**

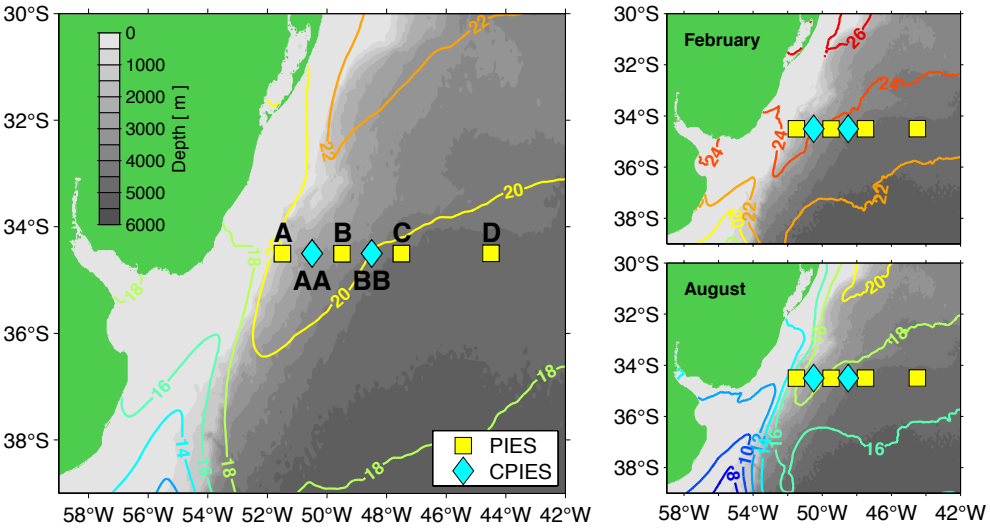

1119 Figure 1: Map illustrating the location of the moored instruments used in this study.
1120 Instrument types are noted in the legend; site names for the original PIES (yellow
1121 squares) are "A" through "D" from west to east; the newer CPIES (cyan diamonds) site
1122 names are "AA" and "BB", also from west to east. Filled contours indicate bottom
1123 topography from the Smith and Sandwell (1997) data set. Color contours indicate the
1124 time-mean sea-surface temperature (°C) from 2009-2015 from the GHRSST MUR
1125 reanalysis SST data product (see Chin et al. 1998; see also
1126 mur.jpl.nasa.gov/multi_resolution_analysis.php). The smaller panels on the right show
1127 the monthly mean SST maps from 2009-2015 for February (top) and August (bottom) to
1128 illustrate the latitudinal range through which the Brazil-Malvinas Confluence shifts
1129 during the year.
1130
1131
1132
1133

Ocean Sci. Discuss., doi:10.5194/os-2016-76, 2016
Manuscript under review for journal Ocean Sci.
Published: 17 October 2016

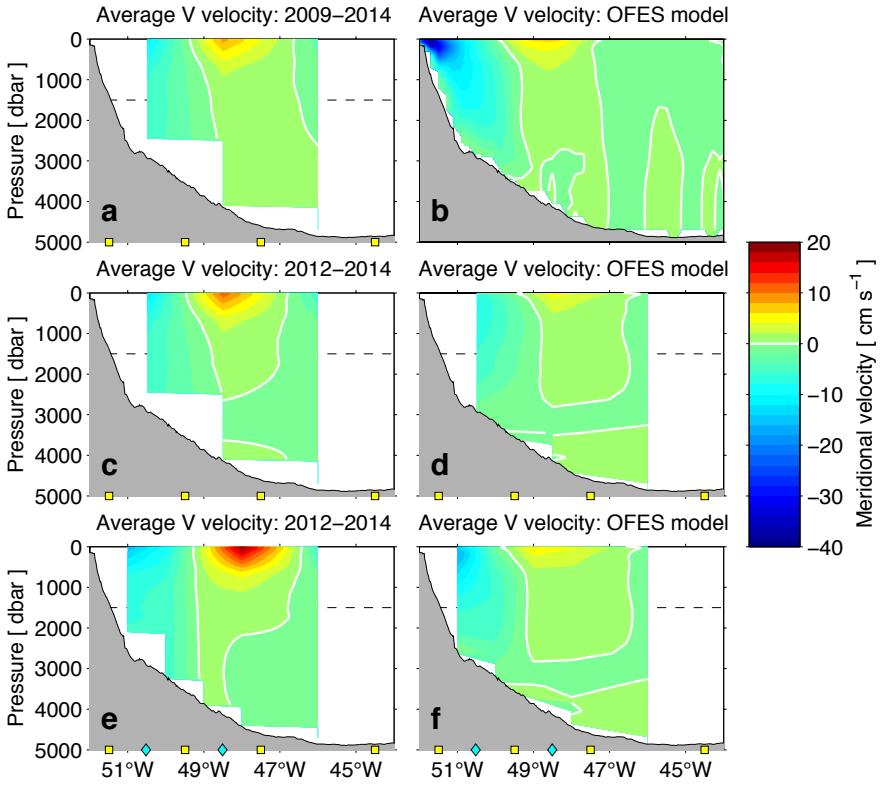

Figure 2: Time-mean meridional velocity from the PIES data (left panels) and from the OFES model (right panels). For the data-based mean sections: top panel indicates the mean over the full 5-year period for which data are available at the four PIES sites (denoted as yellow boxes on bottom axis); middle panel indicates the mean over only the ~2 years when the array was augmented, but still using only the four PIES sites; bottom panel indicates the mean over the augmented ~2 years but now using the additional CPIES sites (denoted as cyan diamonds on bottom axis). For the model-based mean sections: top panel indicates the mean at 0.2° horizontal grid resolution; middle panel indicates the time-mean with the profiles horizontally averaged between the PIES sites; bottom panel indicates the time-mean with the profiles horizontally averaged between all PIES and CPIES sites. For all panels, the gray-filled shape indicates the bottom topography from the Smith and Sandwell (1997) data set. Horizontal dashed line indicates the level where the time-mean from the model is used to reference the bottom-pressure variability.

Ocean Sci. Discuss., doi:10.5194/os-2016-76, 2016
Manuscript under review for journal Ocean Sci.
Published: 17 October 2016

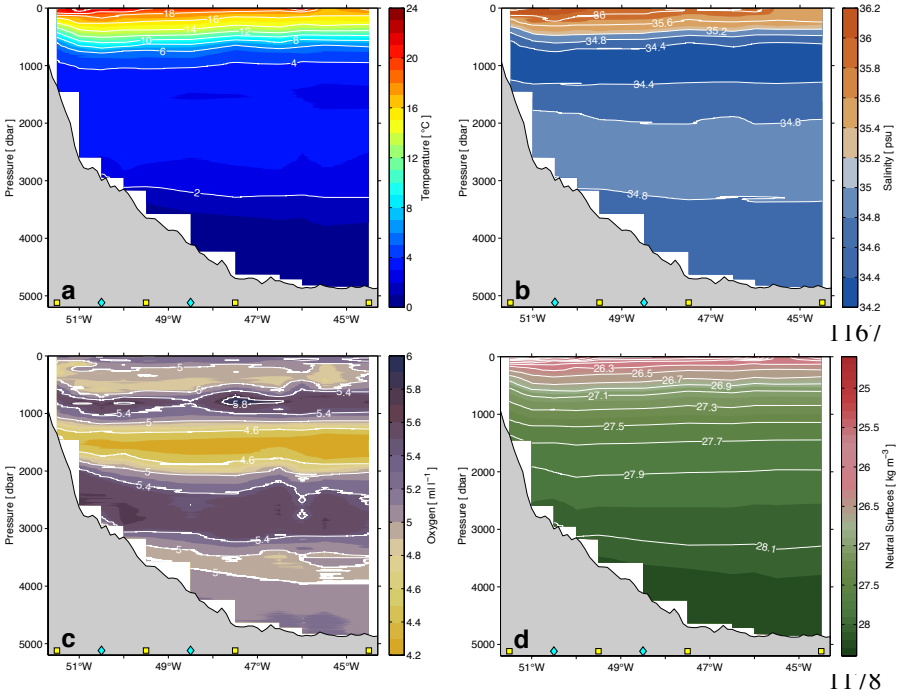

Figure 3: Average sections of in situ temperature (a), salinity (b), dissolved oxygen (c), and neutral density (d). Sections from July 2010, December 2010, July 2011, and December 2012 are averaged in a simple manner to make these plots solely to illustrate the approximate vertical distribution of the water masses in the region.

Ocean Sci. Discuss., doi:10.5194/os-2016-76, 2016
Manuscript under review for journal Ocean Sci.
Published: 17 October 2016

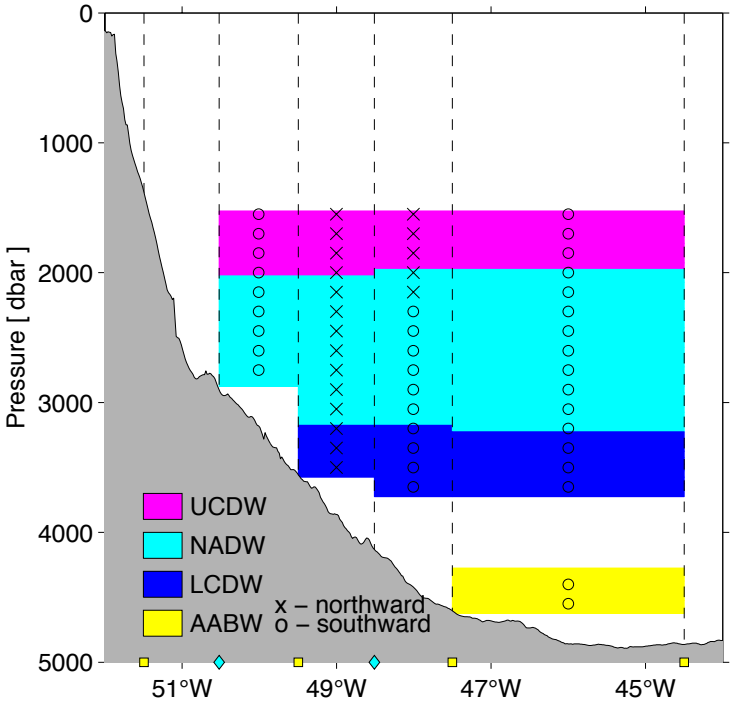

Figure 4: Schematic section illustrating the observed deep water masses and their time-mean flow direction across the section. Water mass definitions are as noted in the text, with the direction of flow denoted with either an "x" or an "o" as noted. Time-mean is determined over the December 2012-October 2014 time period when all six PIES/CPIES sites are available. Water masses are determined using the PIES+GEM estimated profiles. Note the dissolved oxygen criteria for UCDW cannot be tested using the PIES+GEM data, so only the neutral density criteria were employed here; evaluation using the CTD section data suggests that the oxygen criteria is consistently met in the depth range where the UCDW neutral density criteria are satisfied.

Ocean Sci. Discuss., doi:10.5194/os-2016-76, 2016
Manuscript under review for journal Ocean Sci.
Published: 17 October 2016

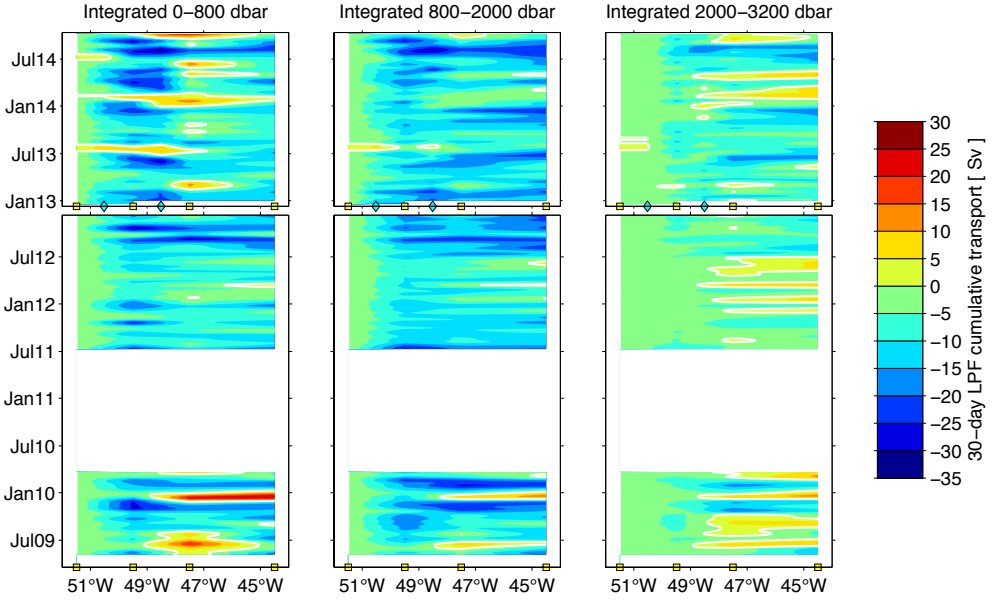

Figure 5: Hovmoller plots illustrating the 30-day low-pass filtered meridional absolute transports integrated in three layers as noted in the panel titles. Transports are cumulatively integrated offshore from the shallowest site eastward toward the center of the basin. Bold white contour indicates zero meridional flow. Symbols along the bottom axes indicate the location of the PIES and CPIES; the upper panels show the time periods when all six sites were available.

Ocean Sci. Discuss., doi:10.5194/os-2016-76, 2016
Manuscript under review for journal Ocean Sci.
Published: 17 October 2016

1217

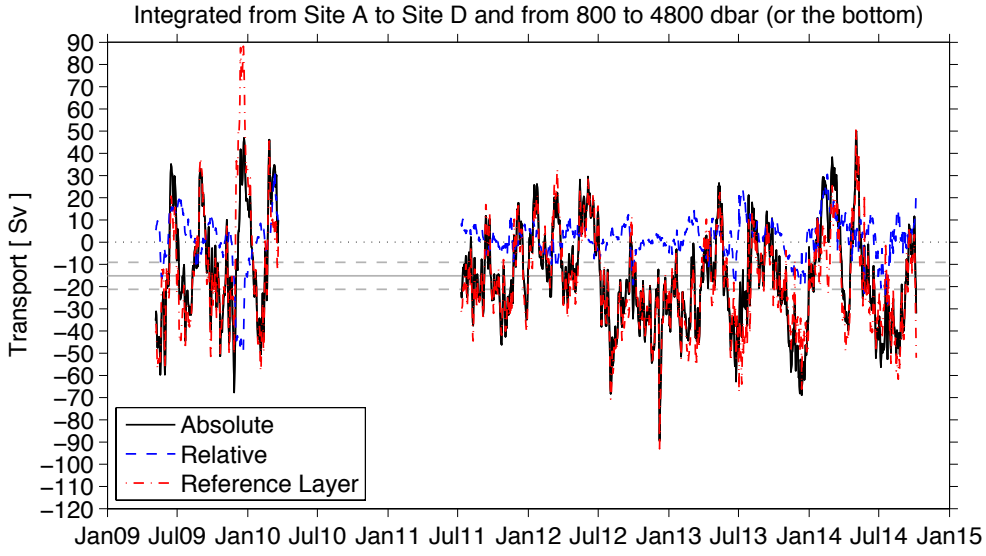

1218
1219
1220 Figure 6: Time series of DWBC volume transport determined across the full horizontal
1221 span of the array and integrated vertically from 800 to 4800 dbar (or the bottom for areas
1222 where it is shallower). The total absolute transport is shown (black solid), as are the
1223 components relative to an assumed level of no motion at 800 dbar ("Relative"; blue
1224 dashed) and associated with the actual reference layer flow ("Reference Layer"; red dash-
1225 dot). The gray horizontal solid and dashed lines respectively indicate the time-mean and
1226 the time-mean plus/minus two standard errors of the mean (i.e. the 95% confidence limit
1227 for the mean value). Standard errors were determined following commonly used
1228 methods (e.g. Dewar and Bane, 1985).
1229
1230
1231
1232
1233
1234

Ocean Sci. Discuss., doi:10.5194/os-2016-76, 2016
Manuscript under review for journal Ocean Sci.
Published: 17 October 2016

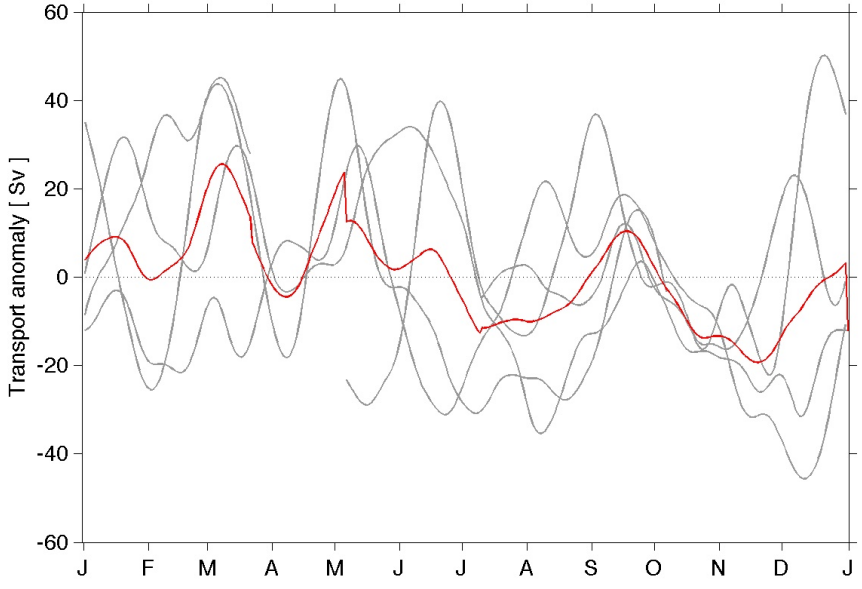

Figure 7: Annual cycle of DWBC volume transport (integrated 800-4800 dbar across the entire array); transport anomalies are shown relative to the record-length mean. Gray lines are individual years; red line is the average of all years. Transport time series was low-pass filtered with a 30-day cutoff period to reduce the higher frequency signals.

Ocean Sci. Discuss., doi:10.5194/os-2016-76, 2016
Manuscript under review for journal Ocean Sci.
Published: 17 October 2016

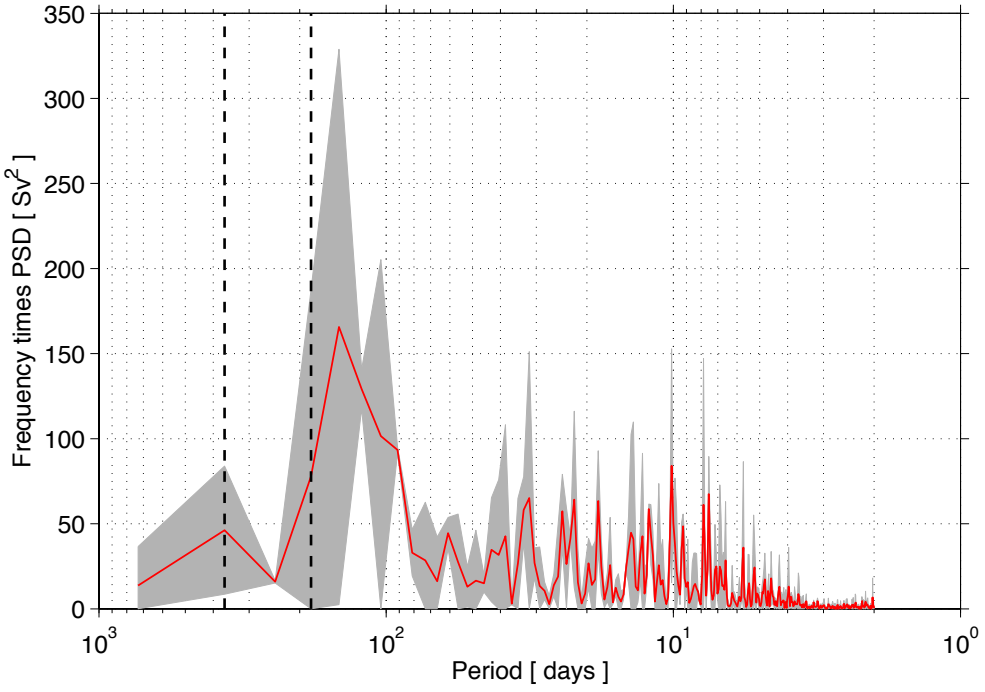

Figure 8: Variance preserving spectrum of the DWBC volume transport using the continuous record that begins in July 2011. Spectrum determined using Welch's averaged periodogram method and a 2-year window allowing 1-year of overlap. Gray shading indicates the 95% confidence limits. Vertical black dashed lines indicate the annual and semi-annual periods.

Ocean Sci. Discuss., doi:10.5194/os-2016-76, 2016
Manuscript under review for journal Ocean Sci.
Published: 17 October 2016

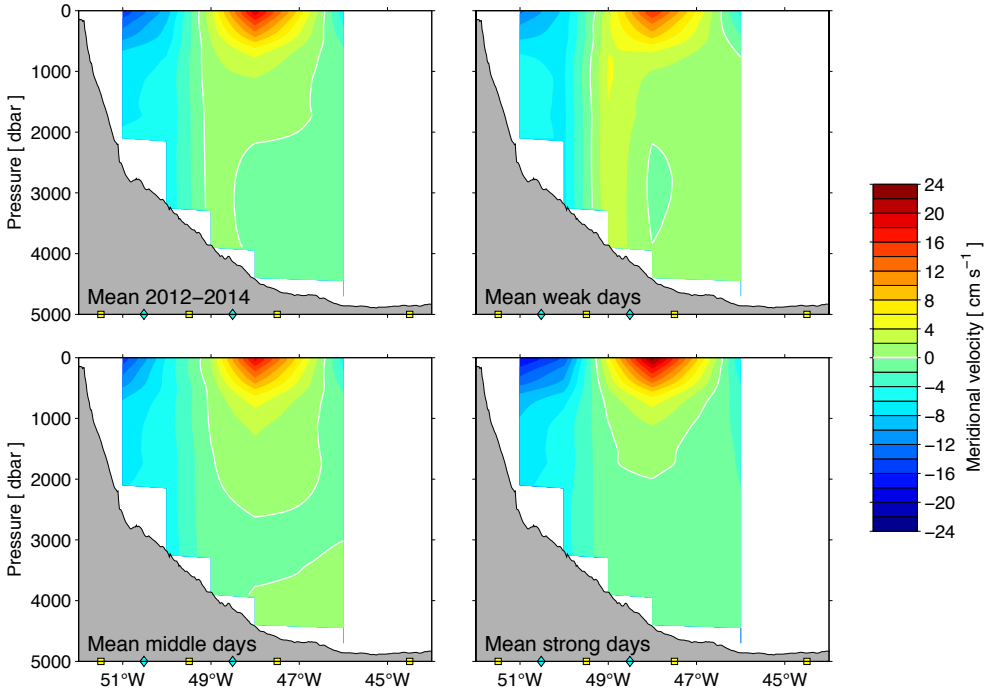

Figure 9: Composite meridional velocity sections based on the average of all data when the enhanced array is in place, December 2012-October 2014 (top left); the average of all days when the southward DWBC transport is within ± 2 standard errors around the mean value ("middle" – lower left); the average of the days where the southward DWBC transport is weaker than the mean minus 2 standard errors ("weak" – top right); and the average of the days where the southward DWBC transport is stronger than the mean plus 2 standard errors ("strong" – lower right). Gray shading indicates bottom topography; symbols along bottom of each panel indicate the PIES and CPIES sites. Note the color bar range is different than for Figure 2.

Ocean Sci. Discuss., doi:10.5194/os-2016-76, 2016
Manuscript under review for journal Ocean Sci.
Published: 17 October 2016

1269

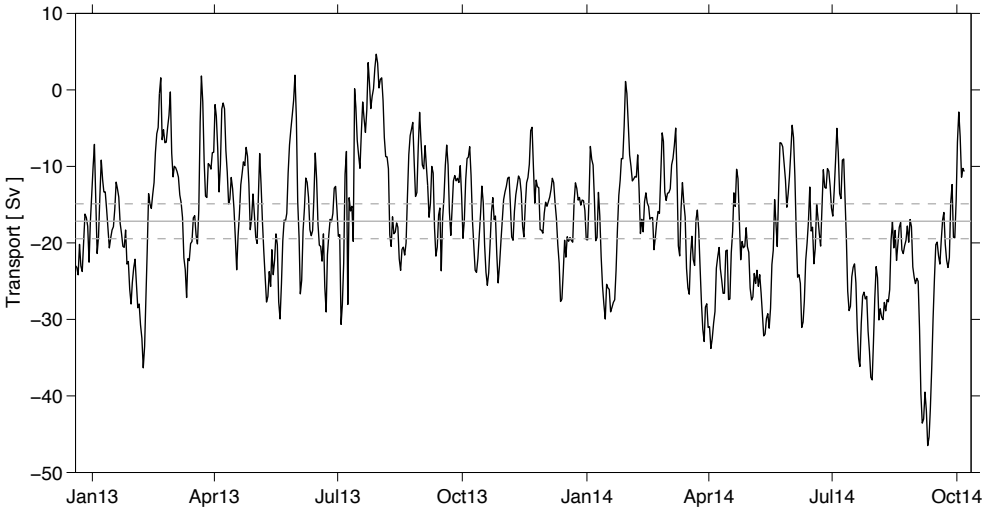

1270
1271
1272 Figure 10: Time series of absolute transport integrated between Sites A and B, and
1273 between 800 dbar and 4800 dbar (or the bottom), during the period when all instruments
1274 were in place. Also shown is the time-mean value (gray solid line) and lines
1275 corresponding to the time-mean plus or minus two standard errors of the mean (gray
1276 dashed), i.e. the 95% confidence limit for the mean value. Standard errors were
1277 determined following commonly used methods (e.g. Dewar and Bane, 1985).
1278
1279
1280
1281
1282

Ocean Sci. Discuss., doi:10.5194/os-2016-76, 2016
Manuscript under review for journal Ocean Sci.
Published: 17 October 2016

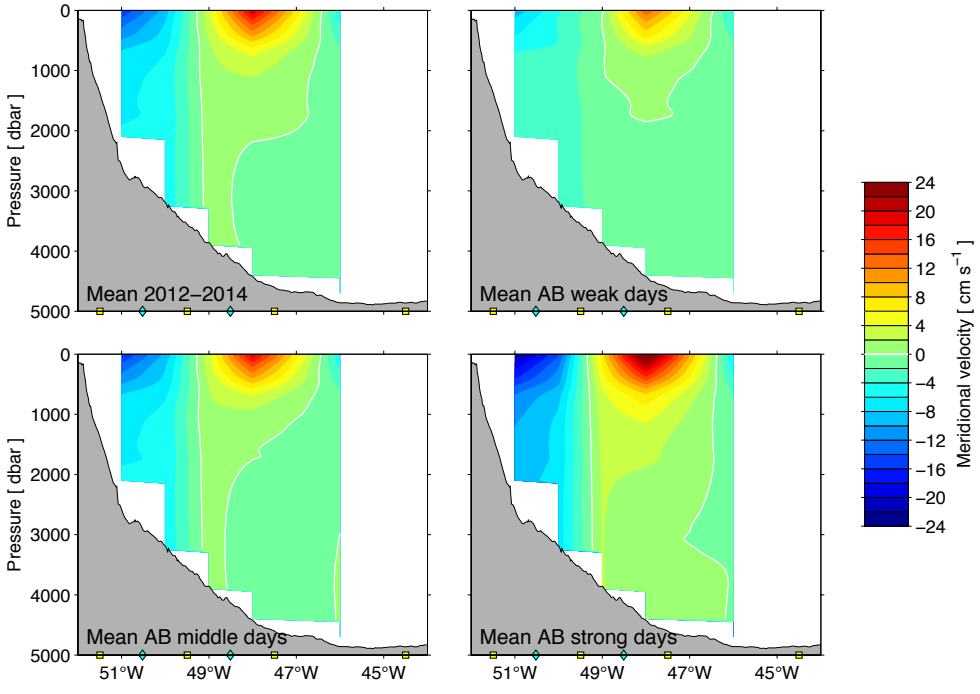

Figure 11: Same as Figure 9, except that the transport time series used for identifying strong and weak southward transport days was integrated only between Sites A and B (i.e. the record in Figure 10) instead of between Sites A and D.

Ocean Sci. Discuss., doi:10.5194/os-2016-76, 2016
Manuscript under review for journal Ocean Sci.
Published: 17 October 2016

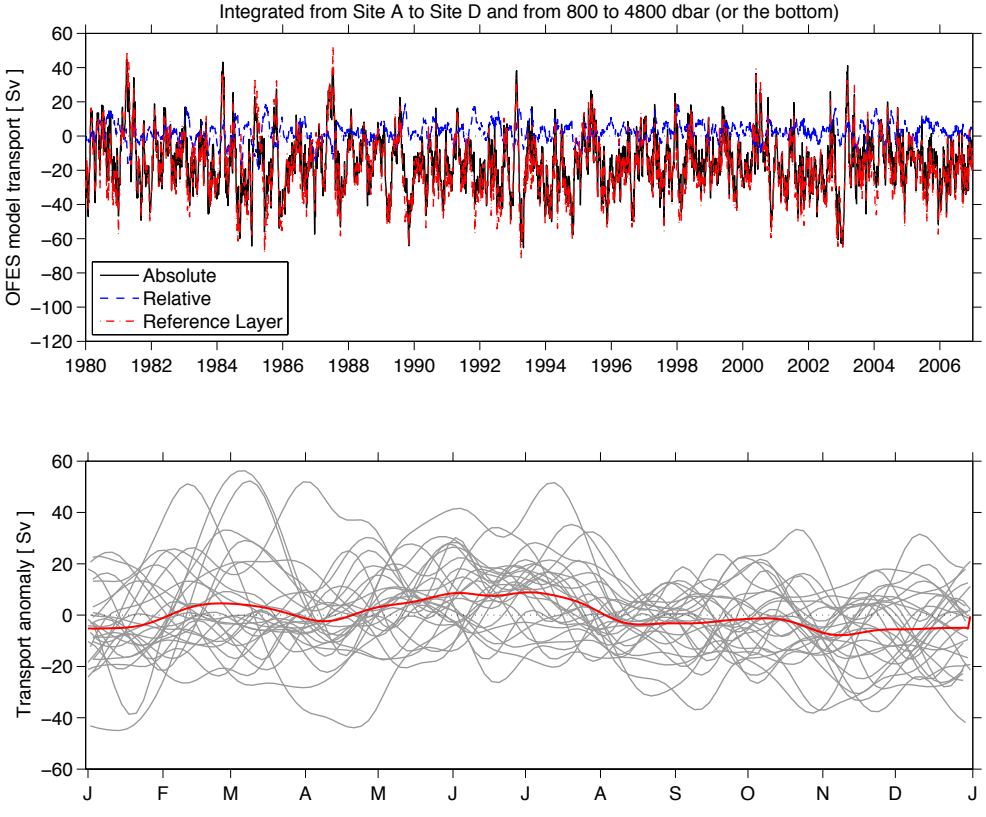

Figure 12: Time series of DWBC volume transport calculated from output of the OFES numerical model run described within the text. Transport was integrated within 800 to 4800 dbar and between the longitudes of the real world PIES at Sites A and D. Top panel: the complete time series of absolute transport, with the every-three-day full resolution, is shown as the black solid line, while the relative and reference contributions calculated as in Figure 6 are shown in blue dashed and red dash-dot lines, respectively. Bottom panel: annual cycle of the model DWBC transport anomaly, calculated and shown in the same manner as for the observational record shown in Figure 7.

Ocean Sci. Discuss., doi:10.5194/os-2016-76, 2016
Manuscript under review for journal Ocean Sci.
Published: 17 October 2016

Ocean Science
Discussions
Open Access
EGU

1304

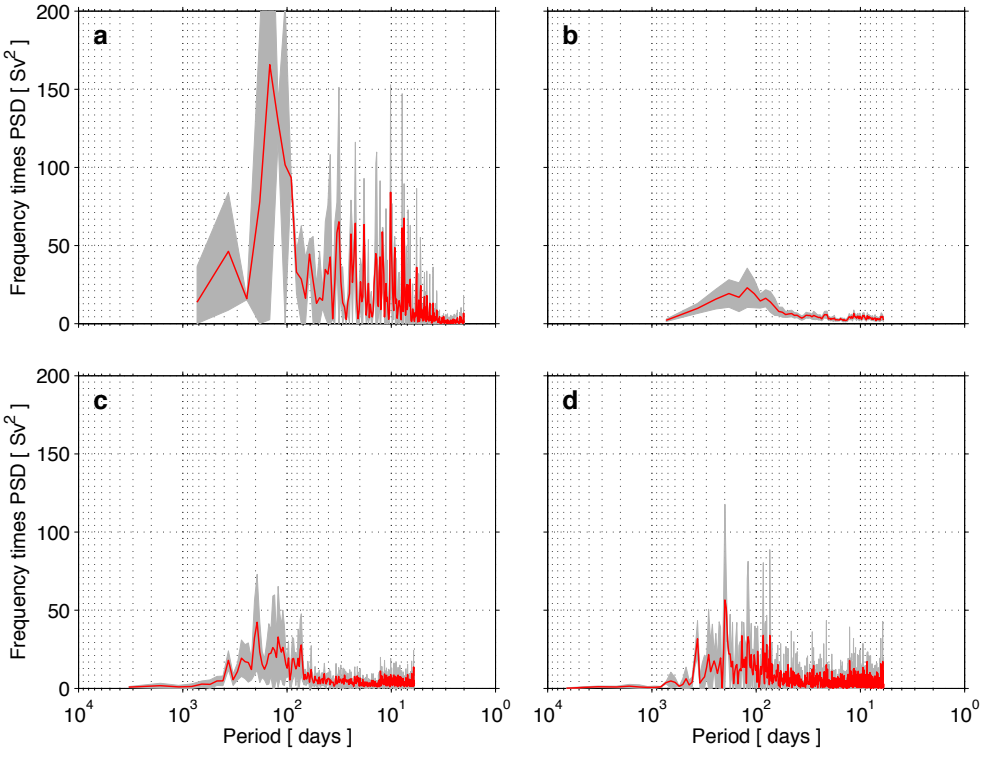

1305
1306
1307 Figure 13: Variance preserving spectra of the DWBC volume transport time series
1308 (integrated from 800 to 4800 dbar and between PIES Sites A and D). a) Spectrum for the
1309 observational record – as in Figure 8 but restricting the y-axis range for comparison
1310 purposes. b) Spectrum for the DWBC transport calculated from the OFES numerical
1311 model output within the same pressure/longitude bounds and utilizing a two-year window
1312 length with 50% window overlap. c) Same as panel b but using a nine-year window
1313 length with 50% window overlap. d) Same as panel b but using an eighteen-year window
1314 length with 50% window overlap. For all panels the gray shaded region represents the
1315 95% confidence limits for the calculated spectrum. All spectra determined using the
1316 Welch's averaged periodogram method.
1317
1318
1319

Ocean Sci. Discuss., doi:10.5194/os-2016-76, 2016
Manuscript under review for journal Ocean Sci.
Published: 17 October 2016

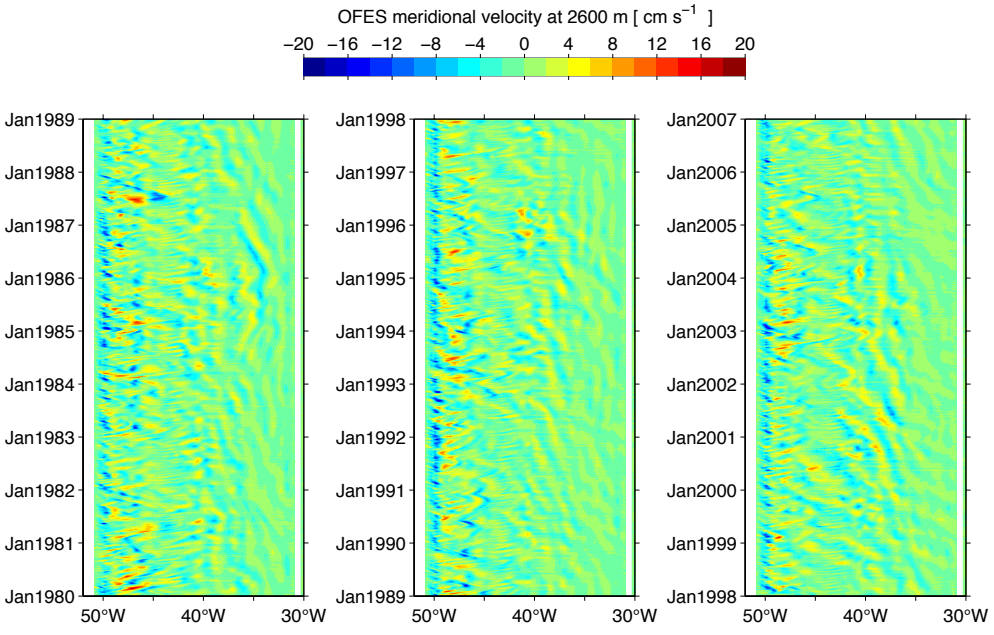

Figure 14: Hovmoller plot illustrating the OFES model meridional velocity along 34.5°S at the core of the NADW near 2600 m depth. Velocities are shown for the final 27 years of the run discussed in the text, broken into three 9-year panels.

Ocean Sci. Discuss., doi:10.5194/os-2016-76, 2016
Manuscript under review for journal Ocean Sci.
Published: 17 October 2016

1333

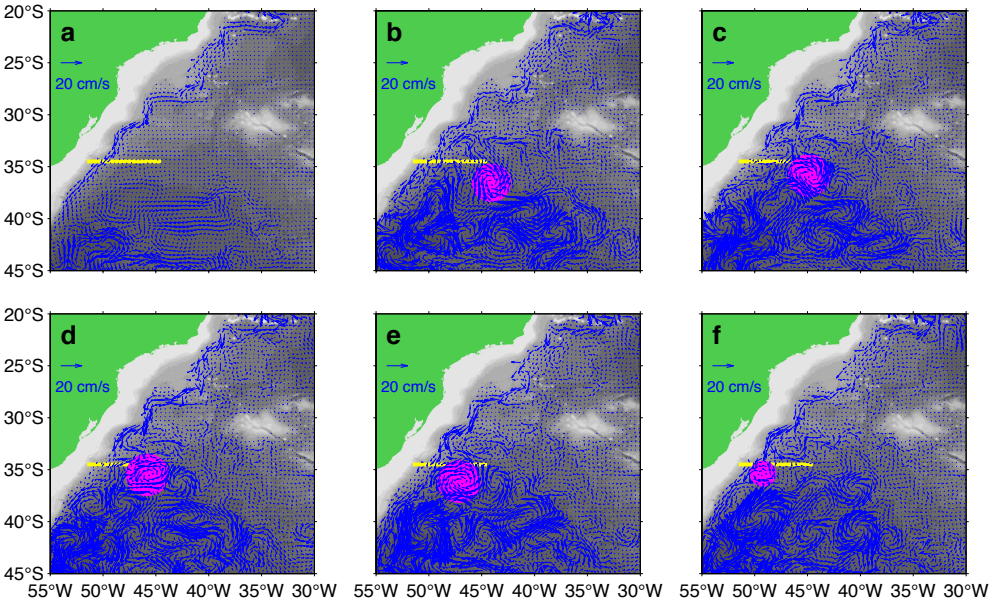

1334
1335
1336 Figure 15: Velocities from the OFES model at the core of the NADW near 2600 m depth:
1337 (a) average over the full 27-year run described in the text; (b) average over August 1987;
1338 (c) average over September 1987; (d) average over October 1987; (e) average over
1339 November 1987; (f) average over December 1987. Land is denoted by green; bottom
1340 topography is from the Smith and Sandwell (1997) data set. Yellow line denotes nominal
1341 location of the PIES/CPIES array in the real ocean. Magenta disc highlights the
1342 propagating eddy/wave feature discussed in the text.
1343
1344
1345